Numerical Analysis of Geosynthetic-Reinforced Soil (GRS) Piers Using Subloading t_{ij} Model

Miles Alexander Drazkowski, Phillip S.K. Ooi and Teruo Nakai

Acknowledgements

- Teruo Nakai
- Tadashi Hashimoto
- Geo-Research Institute
- Yukihiro Morikawa
- Yusaku Isobe
- Hossain Md. Shahin
- Harry Tan Siew Ann
- Hiroomi Takahashi
- Fulbright
- Miles Drazkowski
- Michael Adams
- Jennifer Nicks
- Jonathan Wu
- Landon Kaya
- Melia Talagi

Introduction

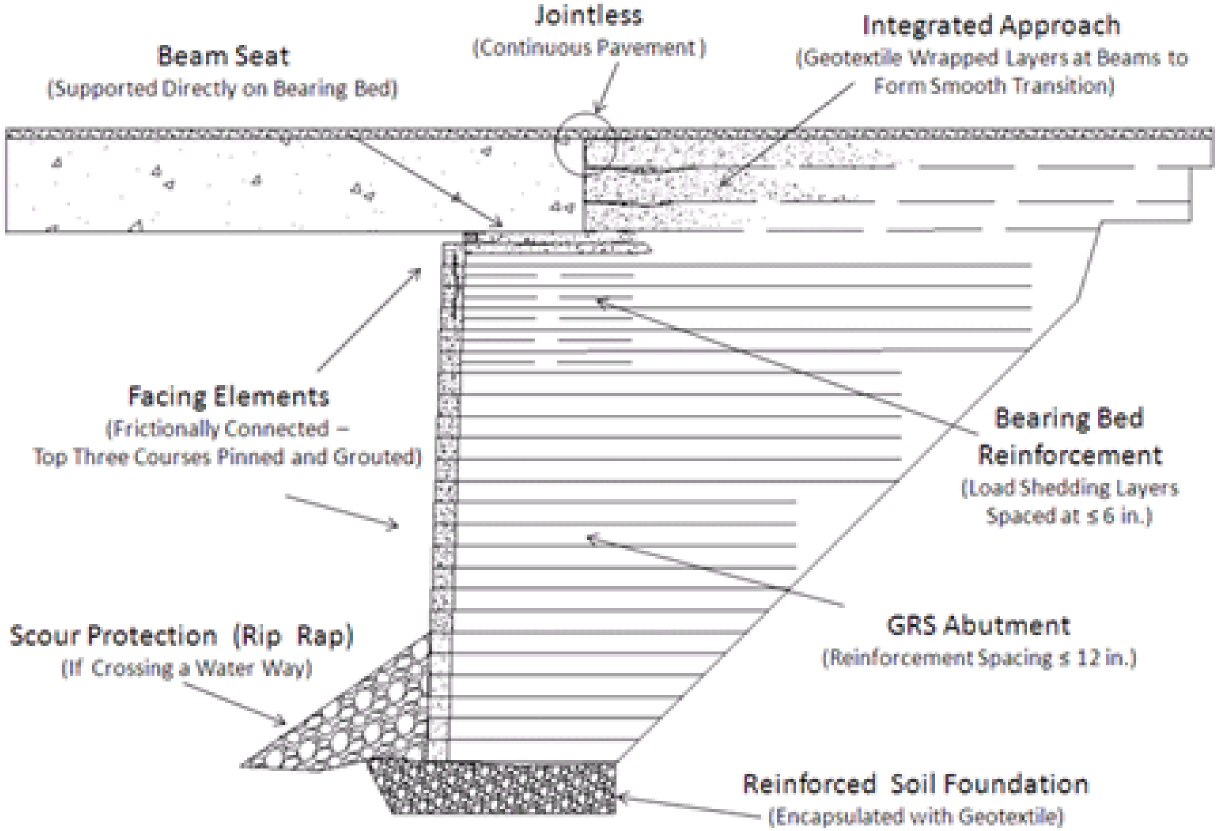

(Adams et al., 2011)

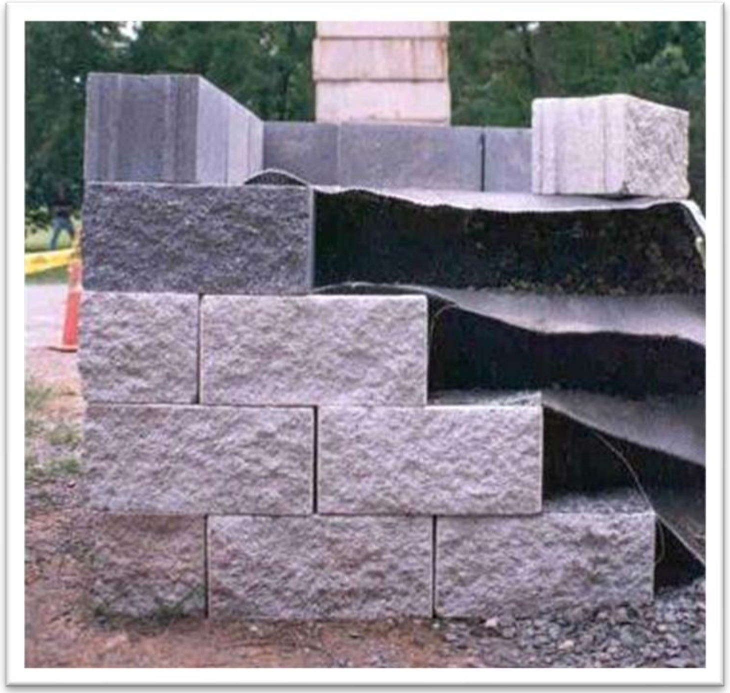

Geosynthetic Reinforced Soil

- Alternating layers of closely spaced (< 30 cm) geosynthetic reinforcement and compacted granular fill

Advantages of GRS-IBS

- Fast/cost-effective – eliminate CIP RC abutment walls/footings – superstructure can be precast
- Reduced carbon footprint – manufacture of 1 ton of cement produces 1 ton CO_2
- Can be built in variable weather using common labor, materials and equipment
- **Quality** compaction control – thin lifts between geosynthetics
- High strength capacity- limit states well understood based on numerous large scale load tests

GRS Mini-Piers

Faced GRS Mini-Pier (Nicks et. al, 2013)

Unfaced GRS Mini-Pier (Nicks et. al, 2013)

- Large scale load tests of GRS mini-piers conducted at FHWA's Turner-Fairbank Highway Research Center, Mclean, VA
- Faced (CMU) and unfaced mini-piers
- 19 tests using hydraulic jack and load frame
- Various reinforcement spacing, geotextile strength, soil type, faced vs unfaced
- Load, and vertical and lateral deformation monitored

Physical Load Tests

- Cost-prohibitive
- Objective – perform numerical load test

Subloading t_{ij} Model Based on Modified Cam Clay

Modified Cam Clay model (Burland and Roscoe, 1968):

Pros

- First elastoplastic model applicable to practical deformation analysis of soil that
  - Can describe soil behavior during shear and consolidation
  - Can model compressive behavior during strain hardening and dilative behavior during strain softening

Cons

- Does not consider effects of σ_2
- e-log p consolidation curve is bilinear instead of curved
- Data shows trace of Hvorslev's yield surface is not planar in principal stress space, but rather curved
- Cannot model dilation during strain hardening nor strain softening of NC clays
- Cannot handle structured behavior of sensitive clays
- etc.

Subloading t_{ij} - Spatially Mobilized Plane

Instead of looking at stresses on octahedral plane, Matsuoka and Nakai (1974) proposed:

- Using stresses on a Spatially Mobilized Plane (SMP)
- SMP coincides with octahedral plane only under isotropic stress conditions (Nakai, 2013).
- SMP is influenced by intermediate principal stress (σ_2)
- SMP is not normal to hydrostatic axis

Matsuoka & Nakai (1974)

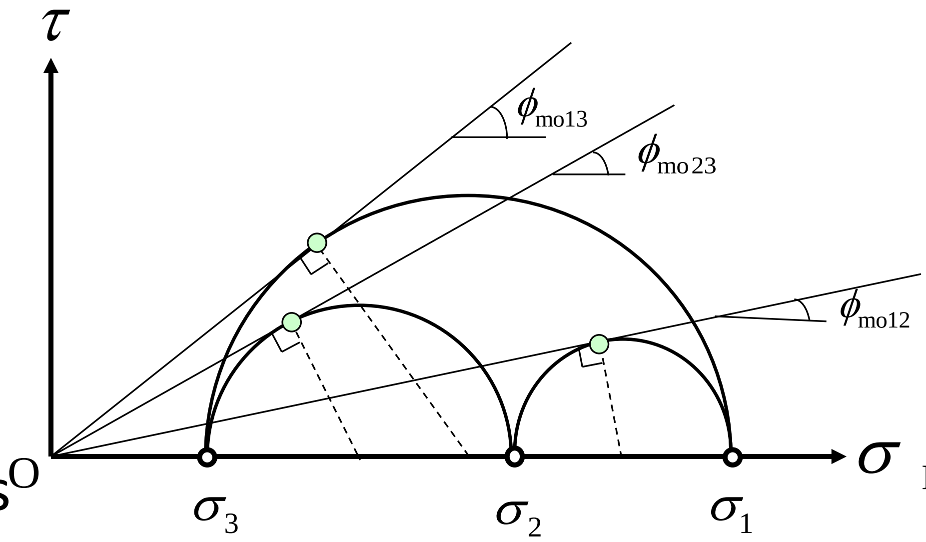

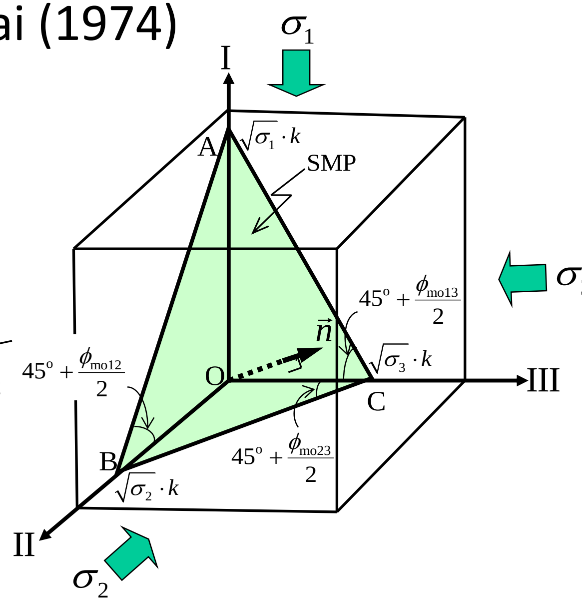

$$tan\left(45^\circ + \frac{\phi_{moij}}{2}\right) = \sqrt{\frac{1\ +\ \sin\phi_{moij}}{1\ +\ \sin\phi_{moij}}} = \sqrt{\frac{\sigma_i}{\sigma_j}}\ (i,j = 1,2,3; i < j)$$

$$I_1 = \sigma_1 + \sigma_2 + \sigma_3$$
$$I_2 = \sigma_1\sigma_2 + \sigma_2\sigma_3 + \sigma_3\sigma_1$$
$$I_3 = \sigma_1\sigma_2\sigma_3$$

$$a_1 = \sqrt{\frac{I_3}{I_2\sigma_1}},\quad a_2 = \sqrt{\frac{I_3}{I_2\sigma_2}},\quad a_3 = \sqrt{\frac{I_3}{I_2\sigma_3}}$$

Subloading t_{ij} Model

Instead of plotting in principal stress space, Nakai and Mihara (1984) plotted in transformed or t_{ij} stress space

- $t_1 = a_1\sigma_1,\ t_2 = a_2\sigma_2,\ t_3 = a_3\sigma_3$ where, (a_1, a_2 and a_3) are direction cosines of normals to SMP

$$a_1 = \sqrt{\frac{I_3}{I_2\sigma_1}}\ ,\ a_2 = \sqrt{\frac{I_3}{I_2\sigma_2}}\ ,\ a_3 = \sqrt{\frac{I_3}{I_2\sigma_3}}$$

- $t_{ij} = a_{ik}\sigma_{kj}$

$$a_{ij} = \sqrt{\frac{I_3}{I_2}} \cdot r_{ij}^{-1} = \sqrt{\frac{I_3}{I_2}} \cdot \left(\sigma_{ik} + I_{r2}\delta_{ik}\right)\left(I_{r1}\sigma_{kj} + I_{r3}\delta_{kj}\right)^{-1}$$

$$(\ r_{ik} r_{kj} = \sigma_{ij}\ )$$

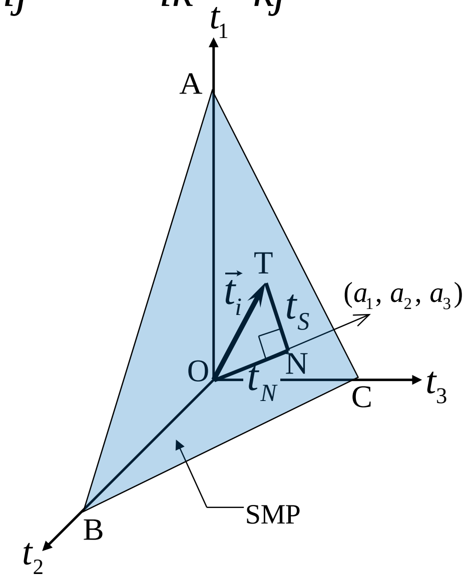

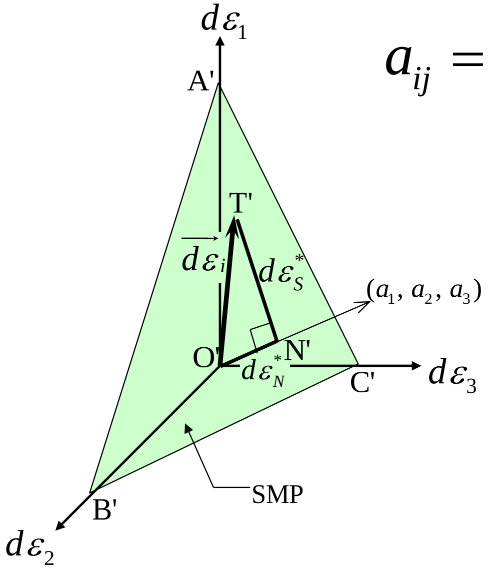

$$\begin{cases} t_N = t_1 a_1 + t_2 a_2 + t_3 a_3 \\ t_S = \sqrt{(t_1 a_2 - t_2 a_1)^2 + (t_2 a_3 - t_3 a_2)^2 + (t_3 a_1 - t_1 a_3)^2} \end{cases}$$

$$\begin{cases} d\varepsilon_N^* = d\varepsilon_1 a_1 + d\varepsilon_2 a_2 + d\varepsilon_3 a_3 \\ d\varepsilon_S^* = \sqrt{(d\varepsilon_1 a_2 - d\varepsilon_2 a_1)^2 + (d\varepsilon_2 a_3 - d\varepsilon_3 a_2)^2 + (d\varepsilon_3 a_1 - d\varepsilon_1 a_3)^2} \end{cases}$$

Subloading t_{ij} Model

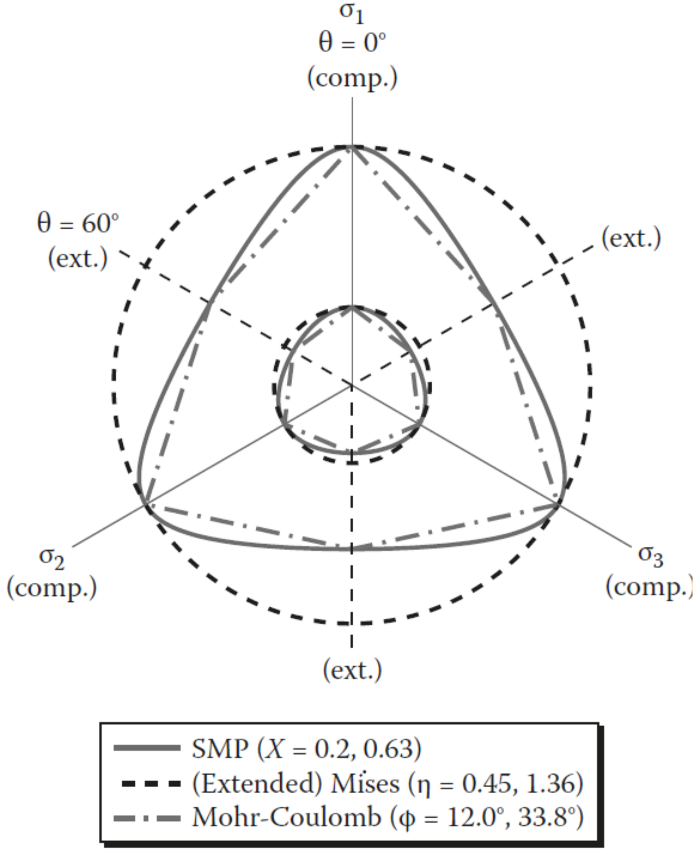

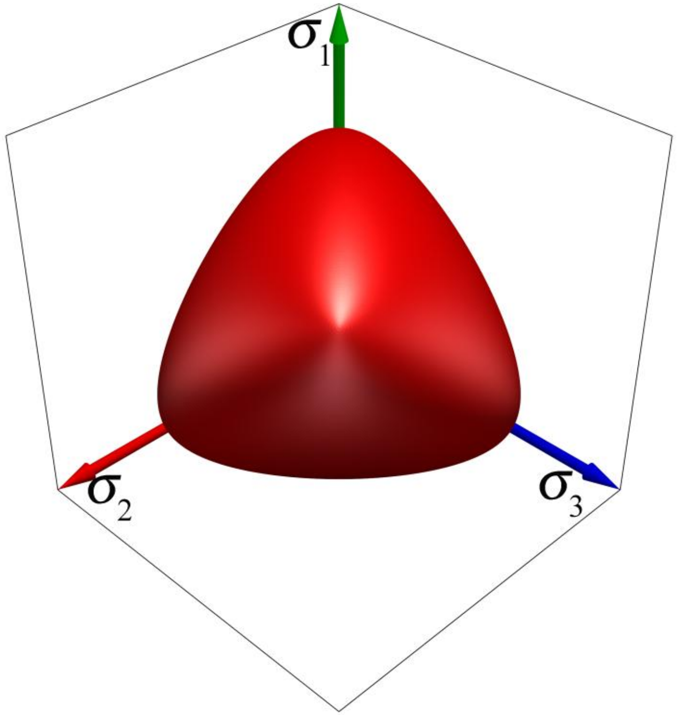

Subloading tij model is a rounded triangle on hydrostatic axis

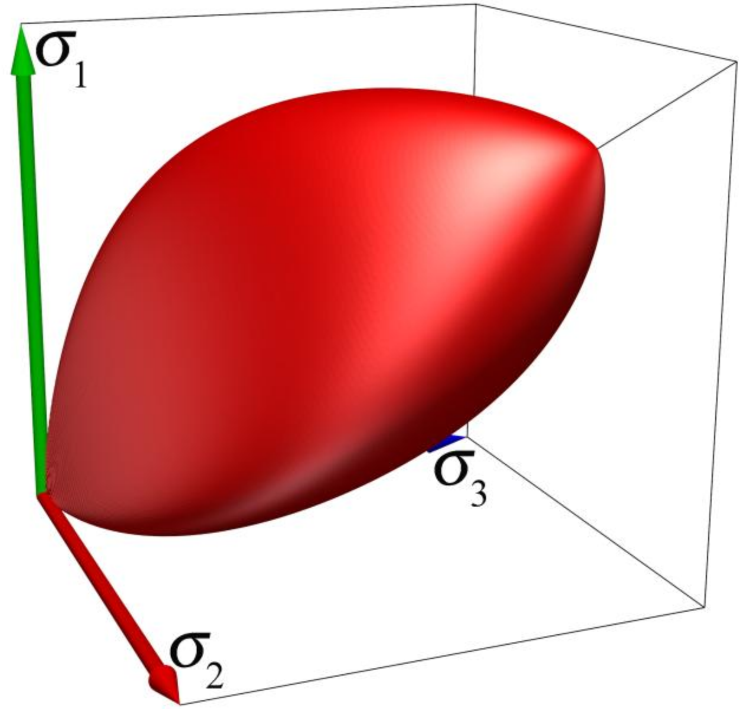

Subloading tij model in σ_1-σ_2-σ_3 space

5 Elements of a Elastoplastic Constitutive Model

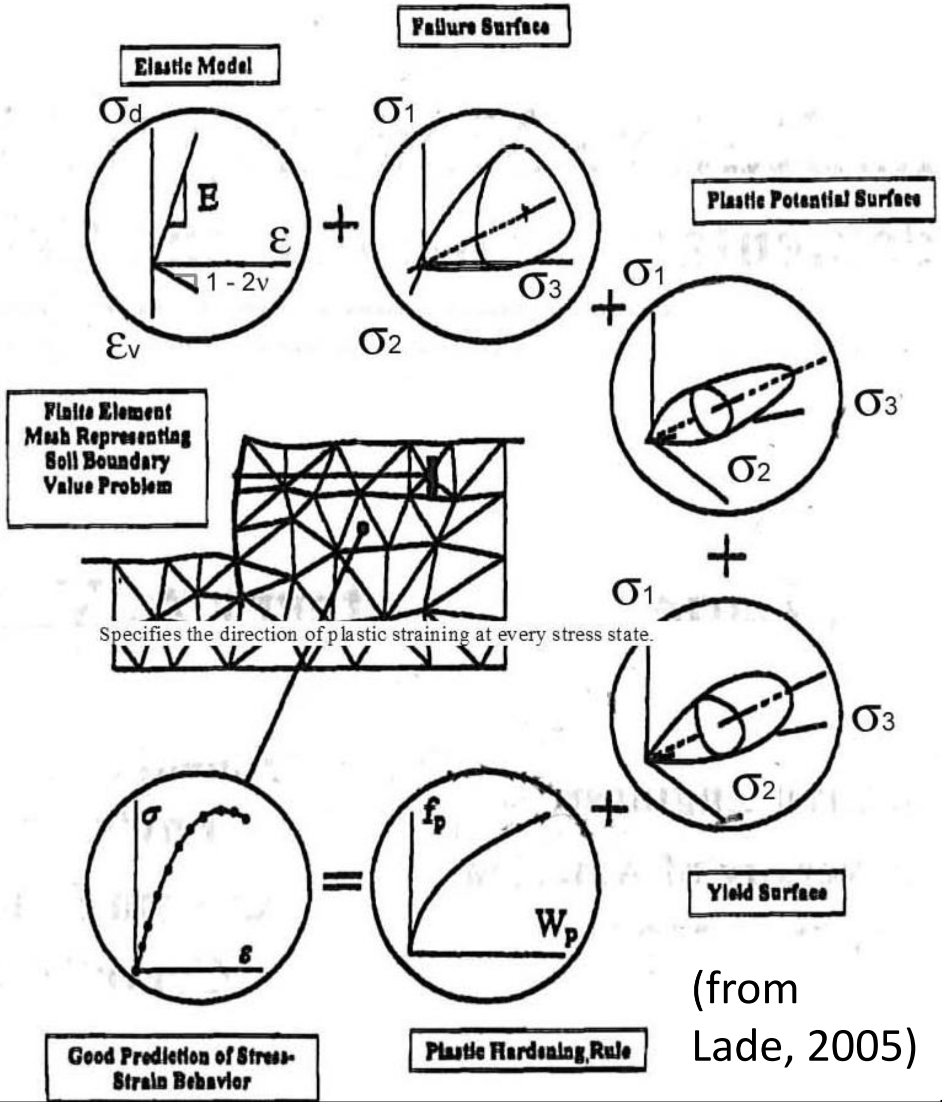

(from Lade, 2005)

	Component	Function
Elastic Behavior	Hooke's Law	Produces elastic strains whenever the stresses change
	Failure Criterion	Imposes limits on stress states that can be reached
Plastic Behavior	Plastic Potential Function	Produces relative magnitudes of plastic strain increments (similar function as Poisson's ratio for elastic strains)
	Yield Criterion	Determines when plastic strain increments occur: Only when yield surface is pushed out/in (hardening/softening)
	Hardening/Softening Relation	Determines magnitudes of plastic strain increments (similar function as Young's modulus for elastic strains)

Elastic Behavior

Expression of elastoplastic model:

$$d\varepsilon_{ij} = d\varepsilon_{ij}^{e} + d\varepsilon_{ij}^{p}$$ see later

$$d\varepsilon_{ij}^{e} = \frac{1+\nu_e}{E_e} d\sigma_{ij} - \frac{\nu_e}{E_e} d\sigma_{mm}\delta_{ij} = C_{ijkl}^{e} d\sigma_{kl}, \qquad E_e = \frac{3(1-2\nu_e)(1+e_0)p}{\kappa}$$

or $\left(d\varepsilon_{ij}^{e} = \frac{1+\nu_e}{E_e} d\left(\frac{\sigma_{ij}}{1+X^2}\right) - \frac{\nu_e}{E_e} d\left(\frac{\sigma_{mm}}{1+X^2}\right)\delta_{ij} = C_{ijkl}^{e} d\sigma_{kl}, \quad E_e = \frac{3(1-2\nu_e)(1+e_0)t_N}{\kappa} \right)$

Failure Criterion

Failure criterion based on SMP (Matsuoka & Nakai,1974)

$$\begin{cases} t_N = t_1 a_1 + t_2 a_2 + t_3 a_3 \\ \quad = \sigma_1 a_1^2 + \sigma_2 a_2^2 + \sigma_3 a_3^2 = 3\dfrac{I_3}{I_2} = \sigma_{SMP} \\ t_S = \sqrt{(t_1 a_2 - t_2 a_1)^2 + (t_2 a_3 - t_3 a_2)^2 + (t_3 a_1 - t_1 a_3)^2} \\ \quad = \sqrt{(\sigma_1 - \sigma_2)^2 a_1^2 a_2^2 + (\sigma_2 - \sigma_3)^2 a_2^2 a_3^2 + (\sigma_3 - \sigma_1)^2 a_3^2 a_1^2} \\ \quad = \dfrac{\sqrt{I_1 I_2 I_3 - 9 I_3^2}}{I_2} = \tau_{SMP} \end{cases}$$

$$\boxed{X = \frac{t_S}{t_N}} = \frac{\tau_{SMP}}{\sigma_{SMP}} = \text{const.} \quad \text{or} \quad \frac{I_3}{I_1 I_2} = \text{const.}$$

Triaxial compression test

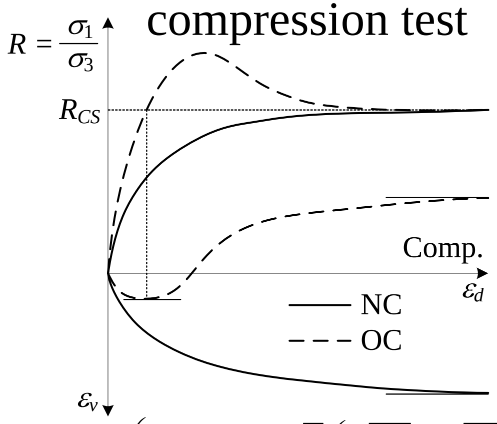

$$\begin{cases} X = \dfrac{t_S}{t_N} = \dfrac{\sqrt{2}}{3}\left(\sqrt{\dfrac{\sigma_1}{\sigma_3}} - \sqrt{\dfrac{\sigma_3}{\sigma_1}}\right) \\ Y = \dfrac{d\varepsilon_N^{*p}}{d\varepsilon_S^{*p}} = \dfrac{1 + 2\sqrt{\dfrac{\sigma_1}{\sigma_3}} \cdot \dfrac{d\varepsilon_3^p}{d\varepsilon_1^p}}{\sqrt{2}\left(\sqrt{\dfrac{\sigma_1}{\sigma_3}} - \dfrac{d\varepsilon_3^p}{d\varepsilon_1^p}\right)} \end{cases}$$

at critical state

$$\begin{cases} \boxed{X_{CS} = \dfrac{\sqrt{2}}{3}\left(\sqrt{R_{CS}} - \dfrac{1}{\sqrt{R_{CS}}}\right)} \\ Y_{CS} = \dfrac{1 - \sqrt{R_{CS}}}{\sqrt{2}\left(\sqrt{R_{CS}} + 0.5\right)} \end{cases}$$

Associated Plasticity: Yield Function = Plastic Potential Function

- $\boxed{f = F - H - \frac{1}{\lambda - \kappa}(\rho_0 - \rho) = 0}$

$$\left\{\begin{array}{l} F = \ln\frac{t_{N1}}{t_{N0}} = \ln\frac{t_N}{t_{N0}} + \varsigma(X), \quad \varsigma(X) = \frac{1}{\beta}\left(\frac{X}{\mathrm{M}^*}\right)^{\beta} \\ \quad\left(\text{where } X = t_s / t_N\right) \\ H = \frac{(-\Delta e)^p}{\lambda-\kappa} = \frac{1+e_0}{\lambda-\kappa}\varepsilon_v^p \end{array}\right.$$

- $d\varepsilon_{ij}^p = \Lambda\frac{\partial F}{\partial t_{ij}} - L^{(IC)}\frac{dt_N}{t_N}\cdot\frac{\frac{\partial F}{\partial t_{ij}}}{\frac{\partial F}{\partial t_{kk}}} + L^{(IC)}\frac{dt_N}{t_N}\cdot\frac{\delta_{ij}}{3} = \left\{\frac{dF}{h^p} - L^{(IC)}\frac{dt_N}{t_N\frac{\partial F}{\partial t_{kk}}}\right\}\frac{\partial F}{\partial t_{ij}} + L^{(IC)}\frac{dt_N}{t_N}\cdot\frac{\delta_{ij}}{3}$

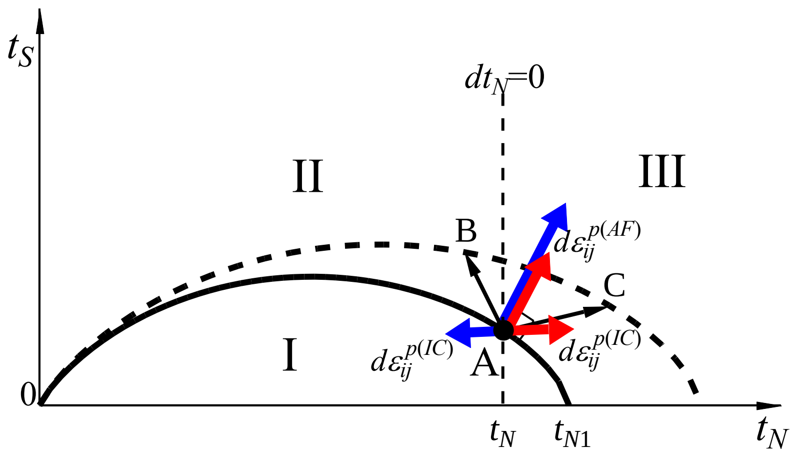

Flow rule considering two components (associated flow and isotropic compression) of plastic strain increment

$$\left(\begin{array}{l} \text{where, } d\varepsilon_v^p = d\varepsilon_{nn}^p = \Lambda\frac{\partial F}{\partial t_{nn}}, \quad L^{(IC)} = \frac{R^{(IC)}}{h^{p(IC)}} = \frac{\left\langle\frac{\partial F}{\partial t_{kk}}\frac{t_N}{\sqrt{3}}\right\rangle^2}{h^{p(IC)}} \\ h^p = \frac{1+e_0}{\lambda-\kappa}\left\{\frac{\partial F}{\partial t_{kk}} + \sqrt{3}\frac{G/(1+k_aX) + Q/(1+k_bX)}{t_N}\right\}, \quad h^{p(IC)} = \frac{1+e_0}{\lambda-\kappa}\left\{1+\left\langle G/(1+k_aX)+Q/(1+k_bX)\right\rangle\right\} \end{array}\right)$$

for both bonding and density effects

Loading $\left\{\begin{array}{ll} d\varepsilon_{ij}^p = d\varepsilon_{ij}^{p(AF)} + d\varepsilon_{ij}^{p(IC)} \neq 0 & \text{if } \Lambda = \frac{dF}{h^p} \geq 0 \\ d\varepsilon_{ij}^p = 0 & \text{otherwise} \end{array}\right.$

Nakai (2022)

Formulation of model based on t_{ij} concept

- Method to determine the shape of yield surface (stress-dilatancy relation)

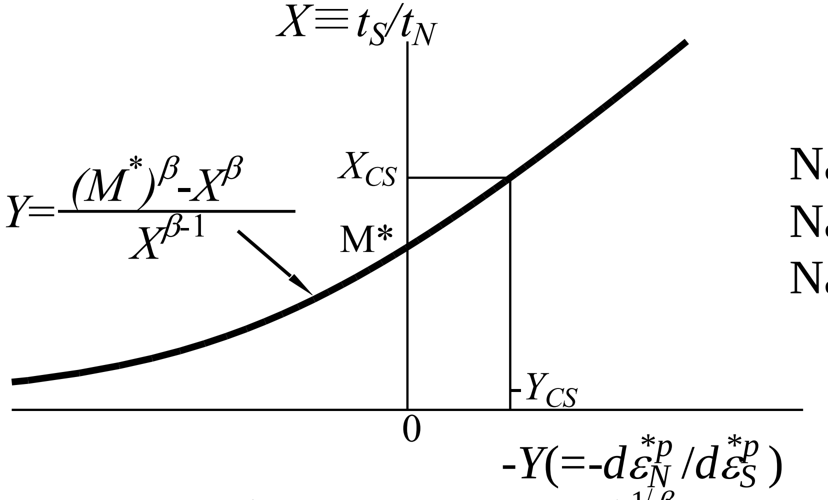

$$M^* = \left(X_{CS}{}^{\beta} + X_{CS}{}^{\beta-1} Y_{CS} \right)^{1/\beta}$$

Nakai and Matsuoka (1986)
Nakai and Hinokio (2004)
Nakai (2013)

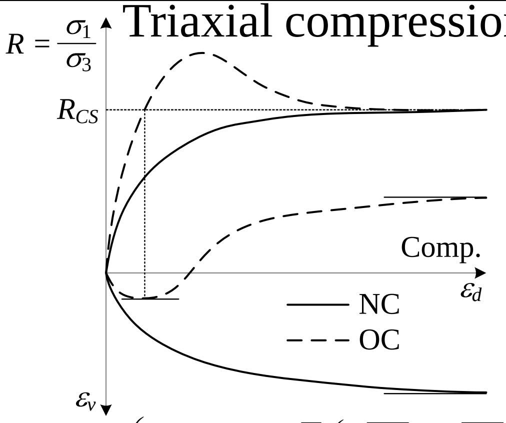

$$\begin{cases} X = \dfrac{t_S}{t_N} = \dfrac{\sqrt{2}}{3}\left(\sqrt{\dfrac{\sigma_1}{\sigma_3}} - \sqrt{\dfrac{\sigma_3}{\sigma_1}}\right) \\ Y = \dfrac{d\varepsilon_N^{*p}}{d\varepsilon_S^{*p}} = \dfrac{1+2\sqrt{\dfrac{\sigma_1}{\sigma_3}}\cdot\dfrac{d\varepsilon_3^p}{d\varepsilon_1^p}}{\sqrt{2}\left(\sqrt{\dfrac{\sigma_1}{\sigma_3}} - \dfrac{d\varepsilon_3^p}{d\varepsilon_1^p}\right)} \end{cases}$$

$\Downarrow$

At critical state

$$\begin{cases} X_{CS} = \dfrac{\sqrt{2}}{3}\left(\sqrt{R_{CS}} - \dfrac{1}{\sqrt{R_{CS}}}\right) \\ Y_{CS} = \dfrac{1-\sqrt{R_{CS}}}{\sqrt{2}\left(\sqrt{R_{CS}}+0.5\right)} \end{cases}$$

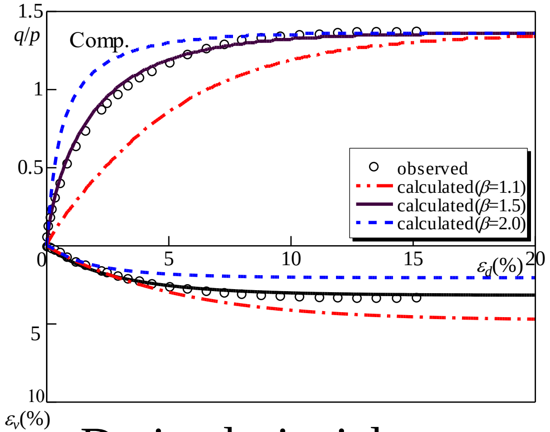

Drained triaxial test

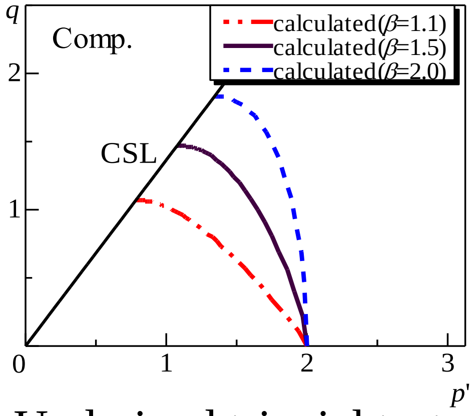

Undrained triaxial test

Hardening Relation

$$\Lambda = \frac{dF}{\frac{1+e_0}{\lambda-\kappa}\left\{\frac{\partial F}{\partial t_{kk}} + \sqrt{3}\,\frac{\frac{G}{(1+k_aX)} + \frac{Q}{(1+k_bX)}}{t_N}\right\}} = \frac{dF}{h^p}$$

$$d\varepsilon_{ij}^p = \frac{dF}{h^p}\cdot\frac{\partial F}{\partial t_{ij}} - L^{(IC)}\frac{dt_N}{t_N}\frac{\frac{\partial F}{\partial t_{ij}}}{\frac{\partial F}{\partial t_{kk}}} + L^{(IC)}\frac{dt_N}{t_N}\frac{\delta_{ij}}{3}$$

$$\left(\begin{array}{l} \text{where, } h^p = \frac{1+e_0}{\lambda-\kappa}\left\{\frac{\partial F}{\partial t_{kk}} + \sqrt{3}\,\frac{\frac{G}{(1+k_aX)} + \frac{Q}{(1+k_bX)}}{t_N}\right\} \\ L^{(IC)} = \frac{R^{(IC)}}{h^{p(IC)}} = \frac{\left\langle \frac{\partial F}{\partial t_{kk}}\frac{t_N}{\sqrt{3}} \right\rangle^m}{h^{p(IC)}} \text{ (usually } m = 2) \\ h^{p(IC)} = \frac{1+e_0}{\lambda-\kappa}\left\{1 + \left\langle \frac{G}{(1+k_aX)} + \frac{Q}{(1+k_bX)} \right\rangle\right\} \end{array}\right)$$

Loading condition:

$$\left(\begin{array}{l} d\varepsilon_{ij}^p \neq 0 \text{ if } \Lambda = \frac{dF}{h^p} > 0 \\ d\varepsilon_{ij}^p = 0 \text{ otherwise} \end{array}\right.$$

GRS Column Setup

TF6

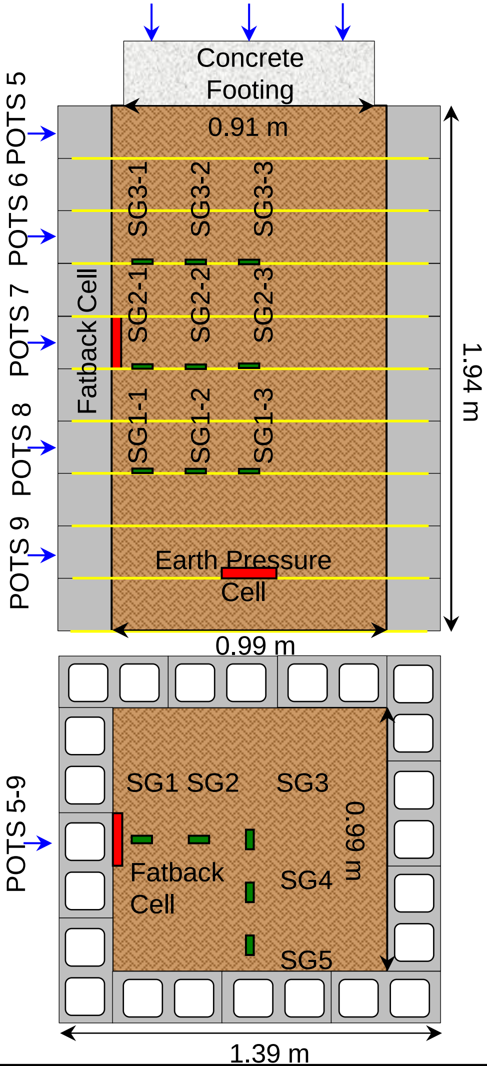

TF7

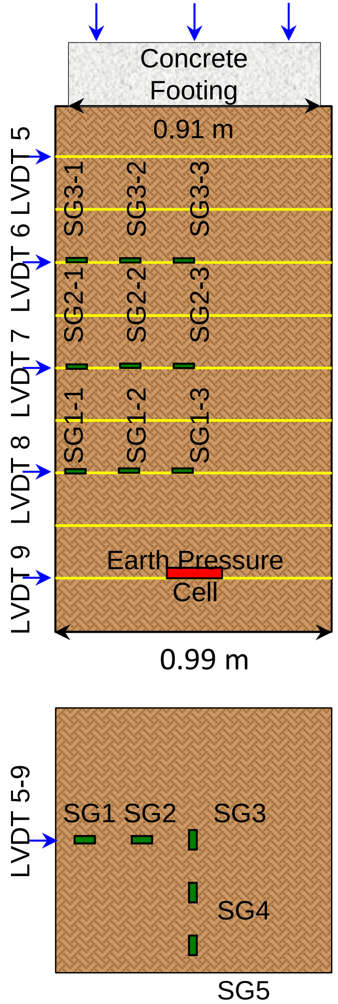

S = 0.194 m

- 0.99 x 0.99 x 1.94 m composite GRS column with alternating layers of granular fill and geosynthetic
- Columns have a 2:1 height-to-width ratio to minimize end effects
- Faced and un-faced columns constructed using same procedure with un-faced having facing removed during final step

TF9

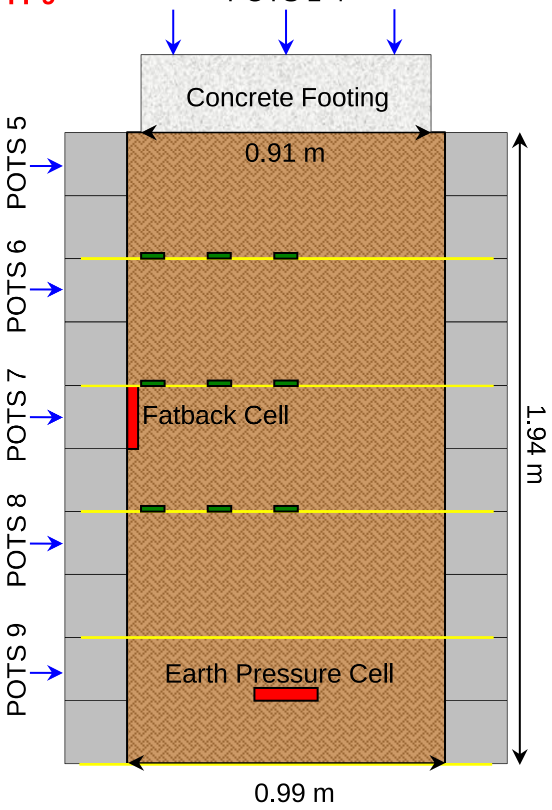

TF10

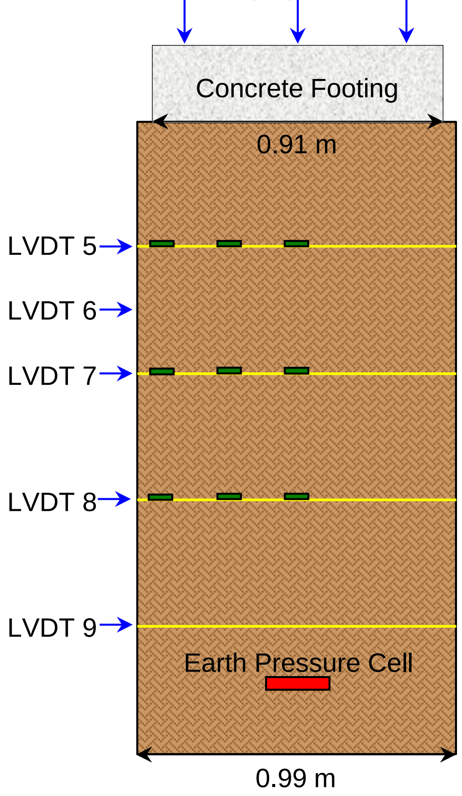

S = 0.389 m

GRS Column Setup

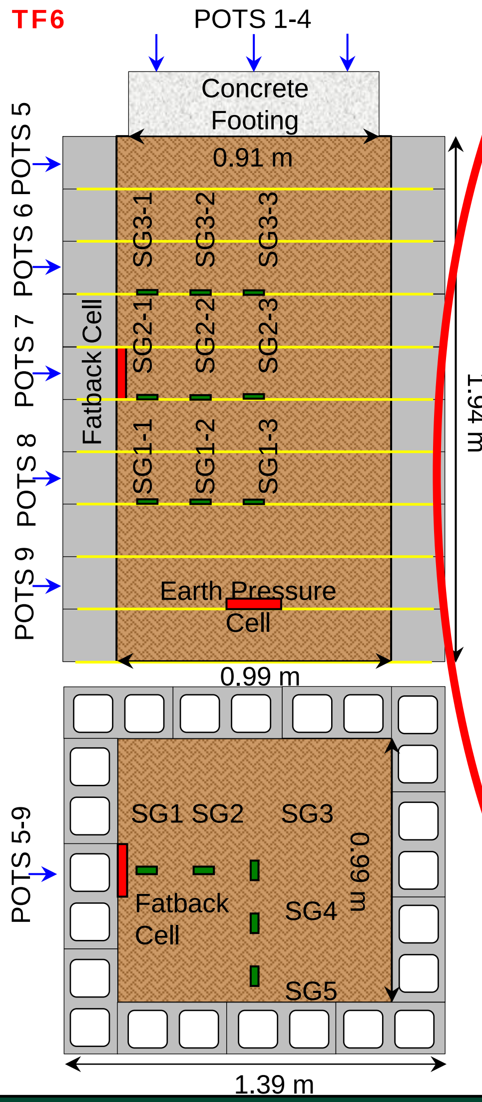

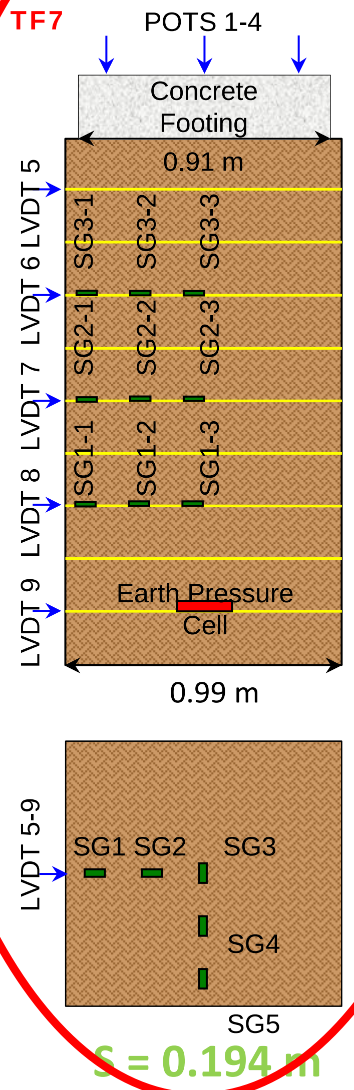

- 0.99 x 0.99 x 1.94 m composite GRS column with alternating layers of granular fill and geosynthetic
- Columns have a 2:1 height-to-width ratio to minimize end effects
- Faced and un-faced columns constructed using same procedure with un-faced having facing removed during final step

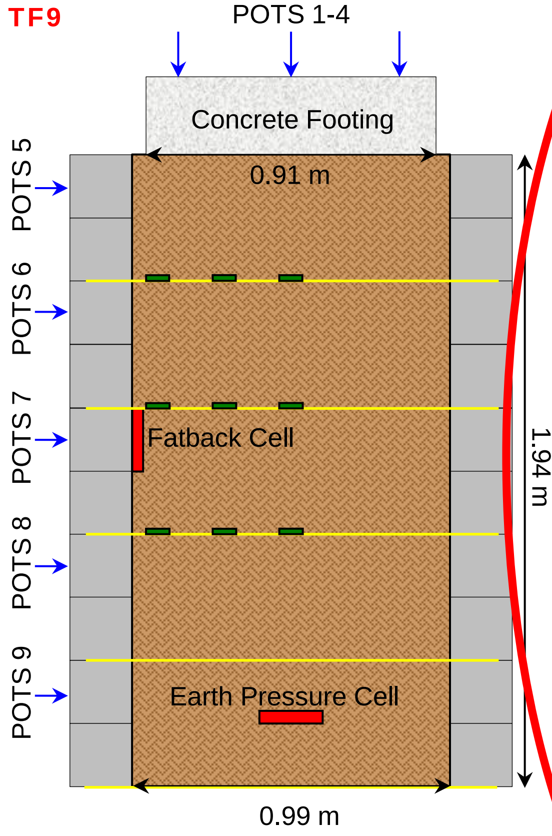

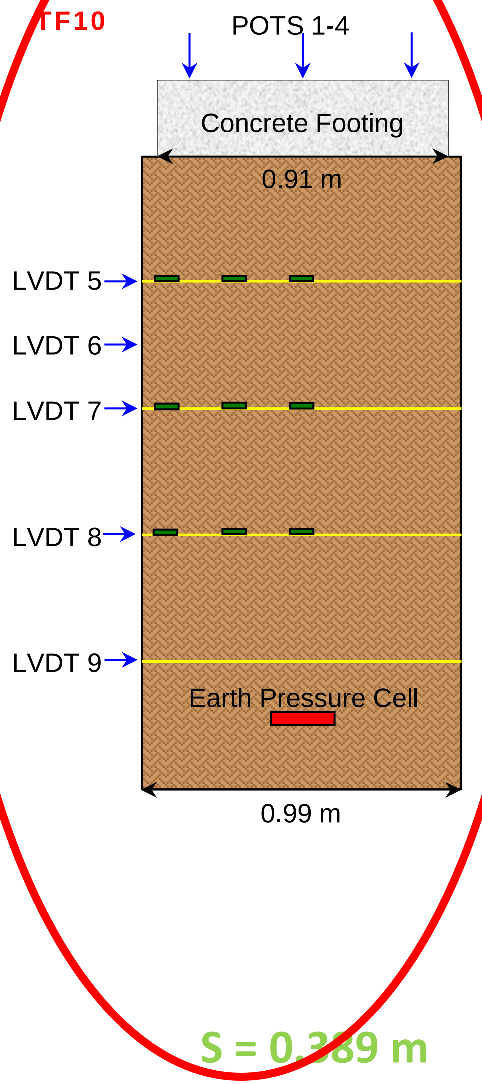

Load Testing

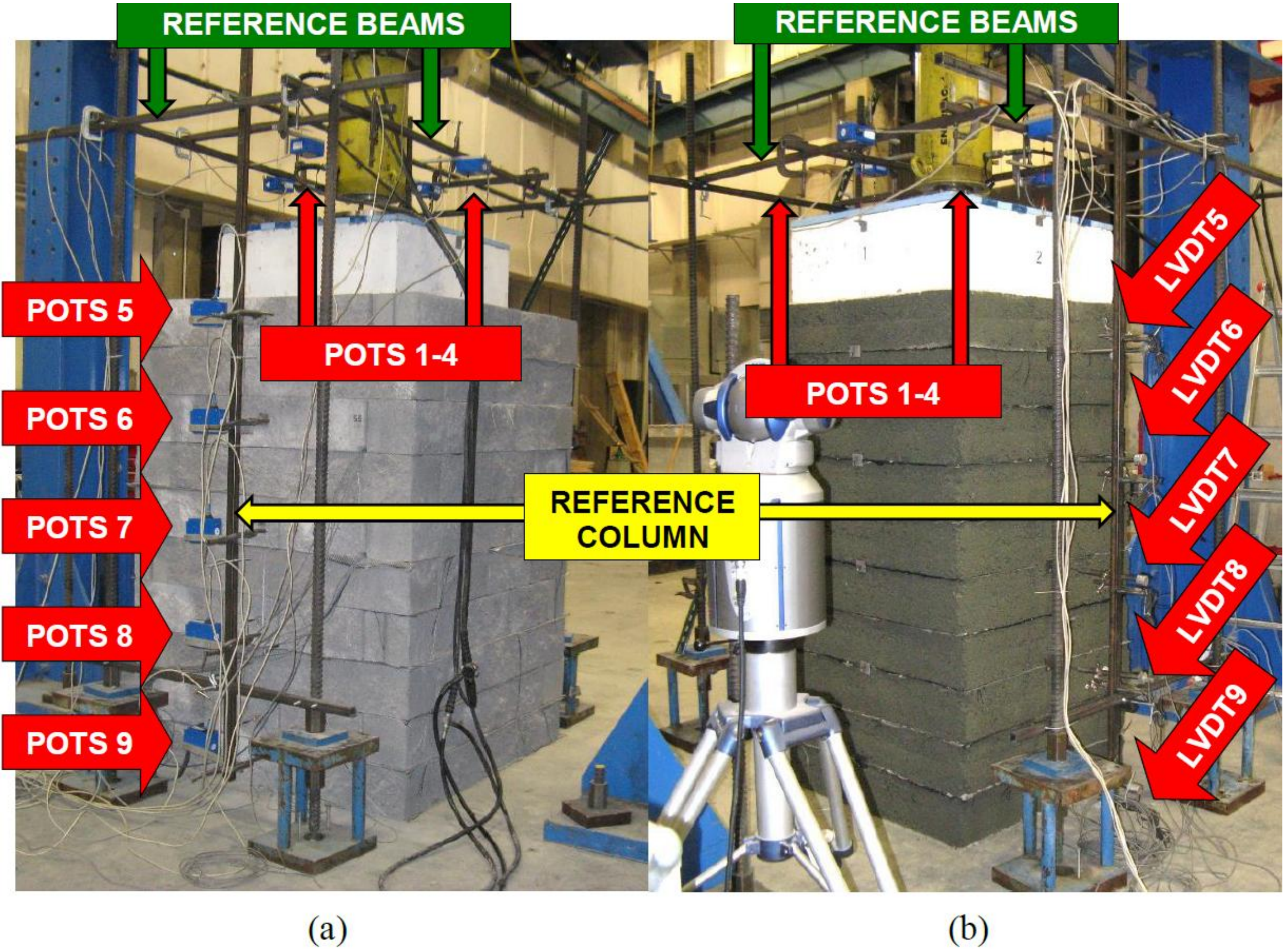

Schematics of deflection instrumentation for mini piers (a) with facing and (b) without facing. (Iwamoto, 2014)

TF-10 at failure with S_v = 15¼ inches, T_f = 4,800 lb/ft, and VDOT 21A material. (Nicks et al., 2013)

Staged Construction

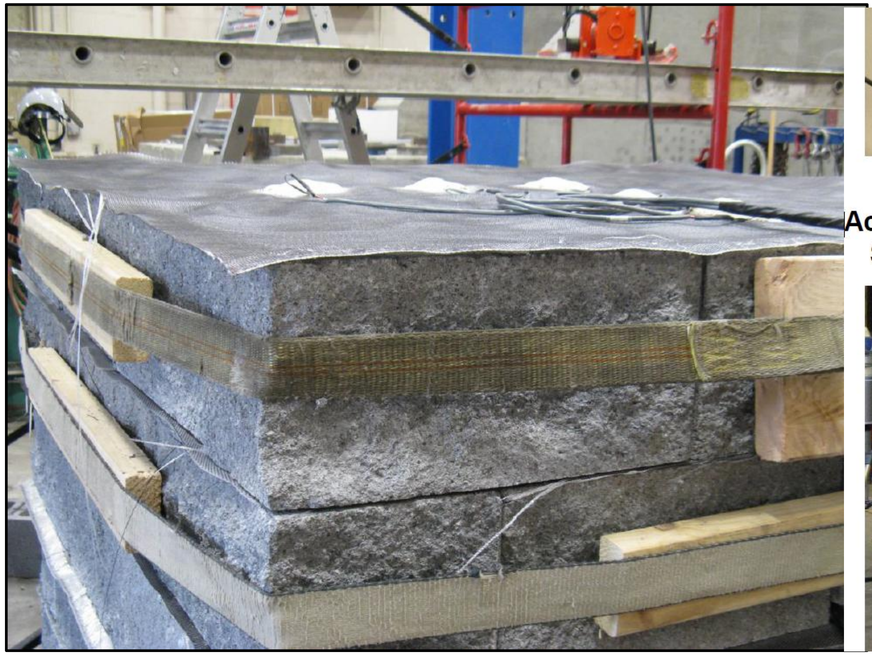

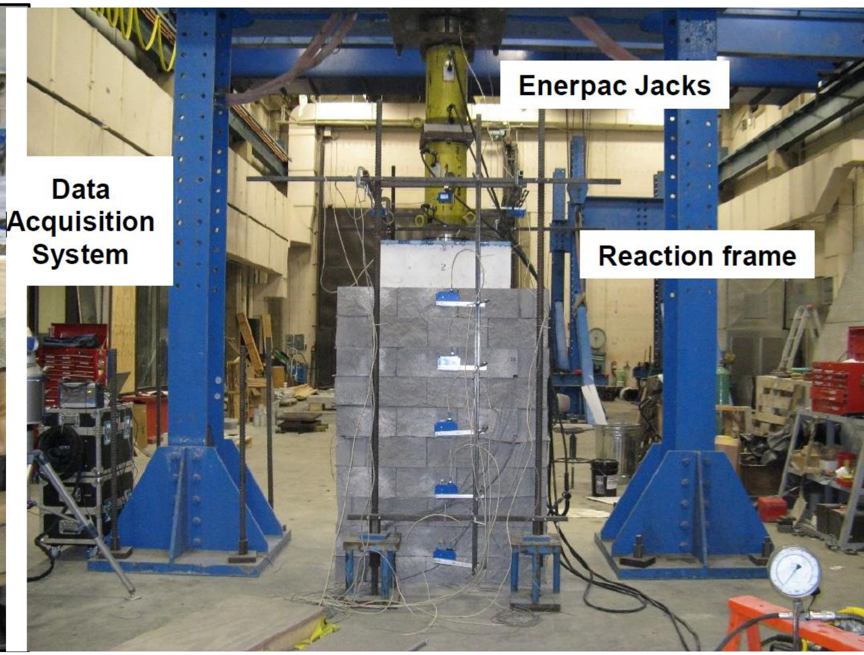

Backfill

Well-graded gravel with silt (GW-GM) from Lucky Stone quarry in Leesburg, VA used as base course

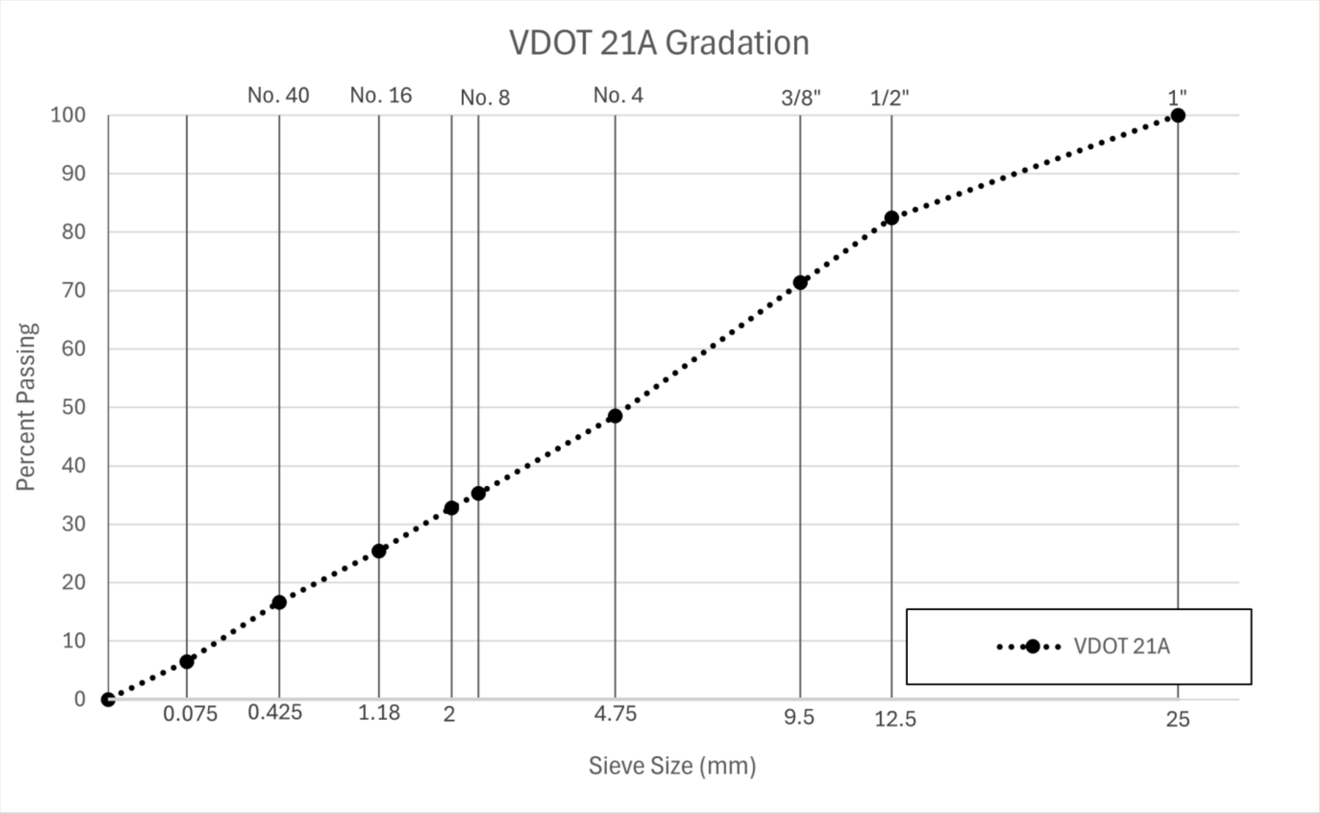

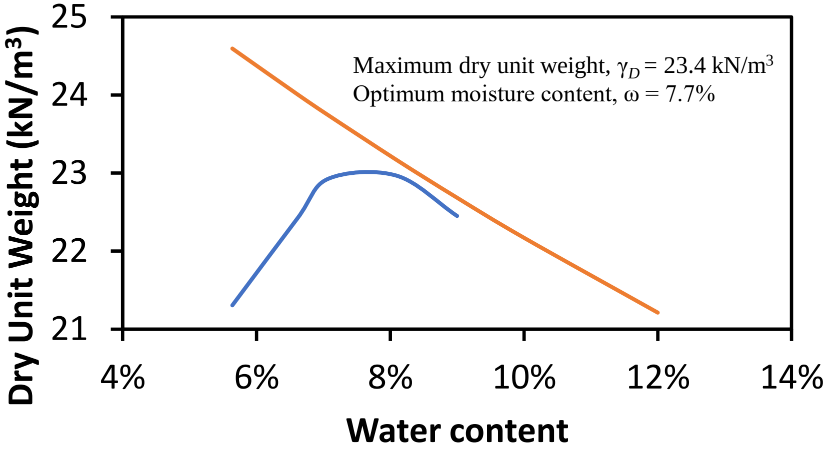

Results of standard Proctor test on the aggregate backfill (Nicks et al., 2013)

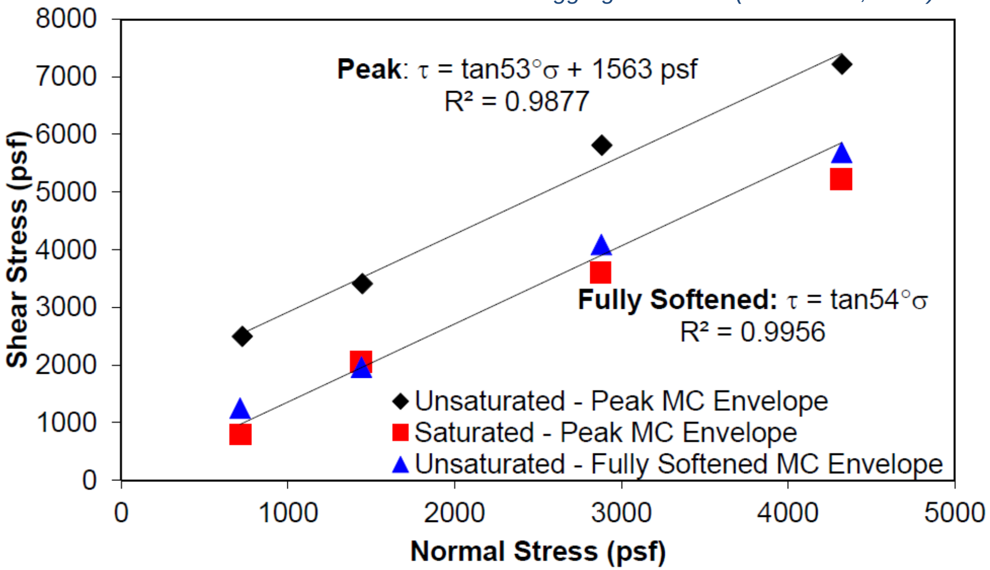

Comparison of saturated, unsaturated, and fully softened Mohr-Coulomb envelopes. (Iwamoto, 2014)

Soil Parameters

Parameter	Value	
λ	0.0325	Same parameters as modified Cam-clay model
κ	0.0016	
$N = e_{NC}$ at 1 atm	0.364	
$R_{CS} = (\sigma_1/\sigma_3)_{CS\ comp}$	5	
ν_e	0.2	
β	1.155	Shape of yield surface
a	400	Influence of density
k_a	10	
b	0	Influence of bonding
$Q_o = b\omega_o$	0	
k_b	0	
e_{max}	0.55	Max. e since p plotted on log scale

Normally consolidated

Over consolidated

Structured clay

Isotropic Consolidation

Modified Cam-clay

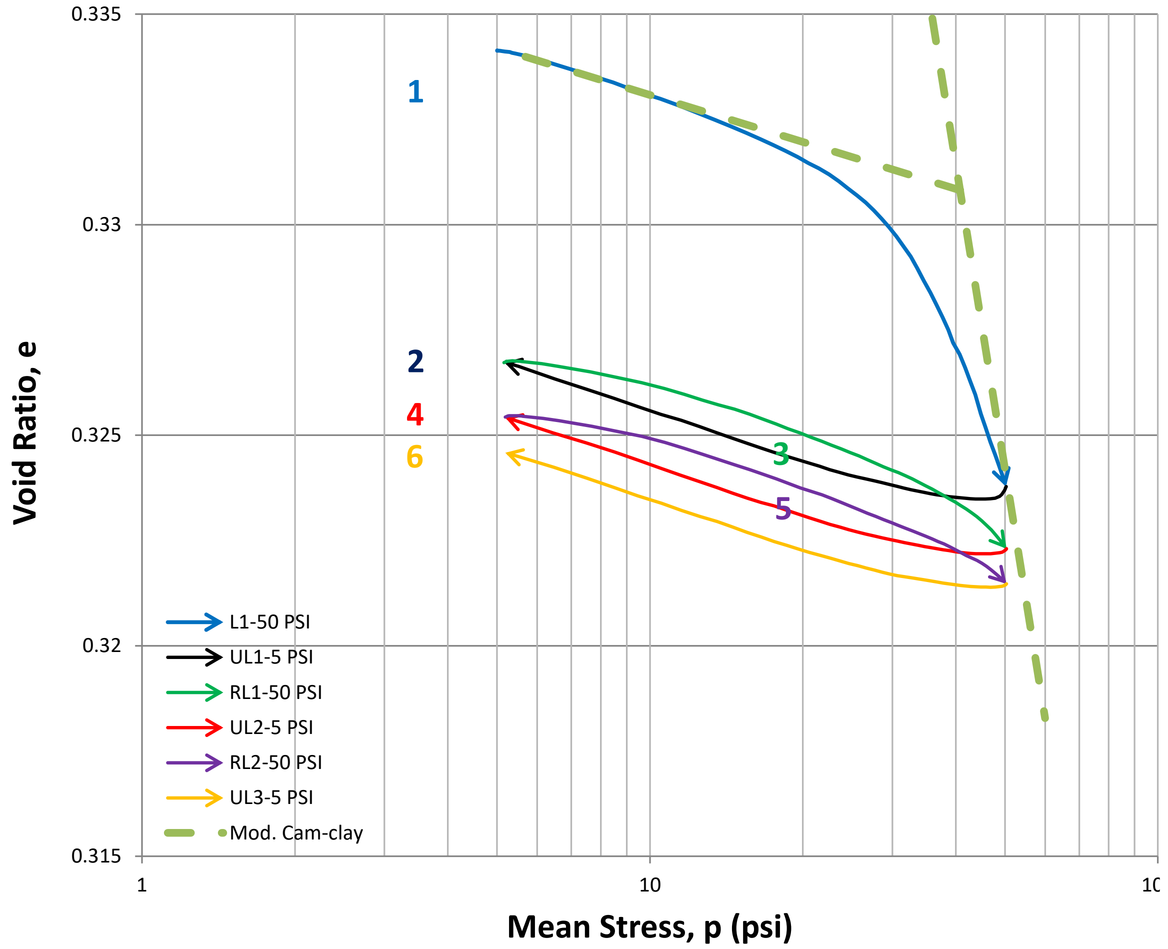

Subloading t_{ij}

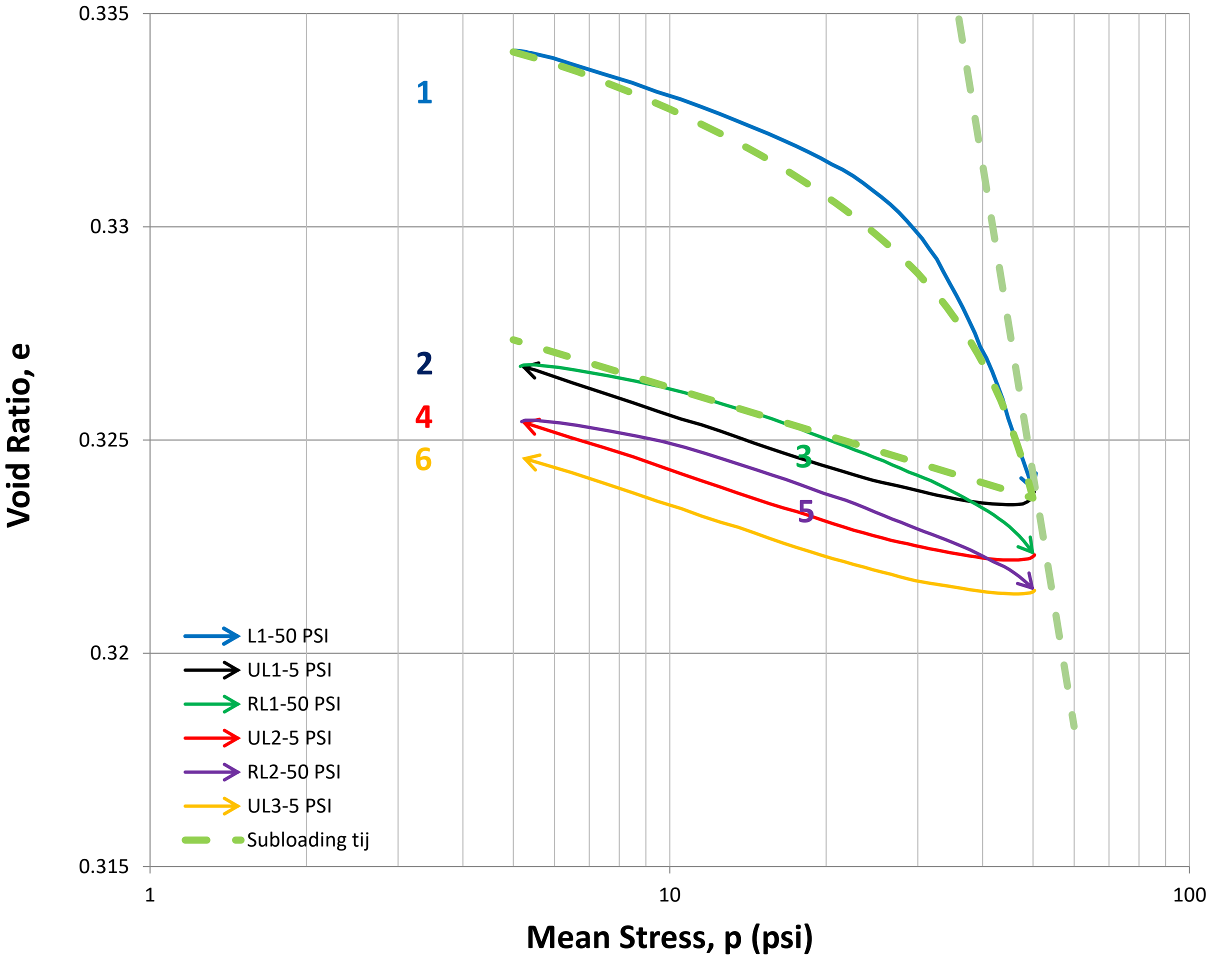

CD Triaxial Test – Model vs Measured

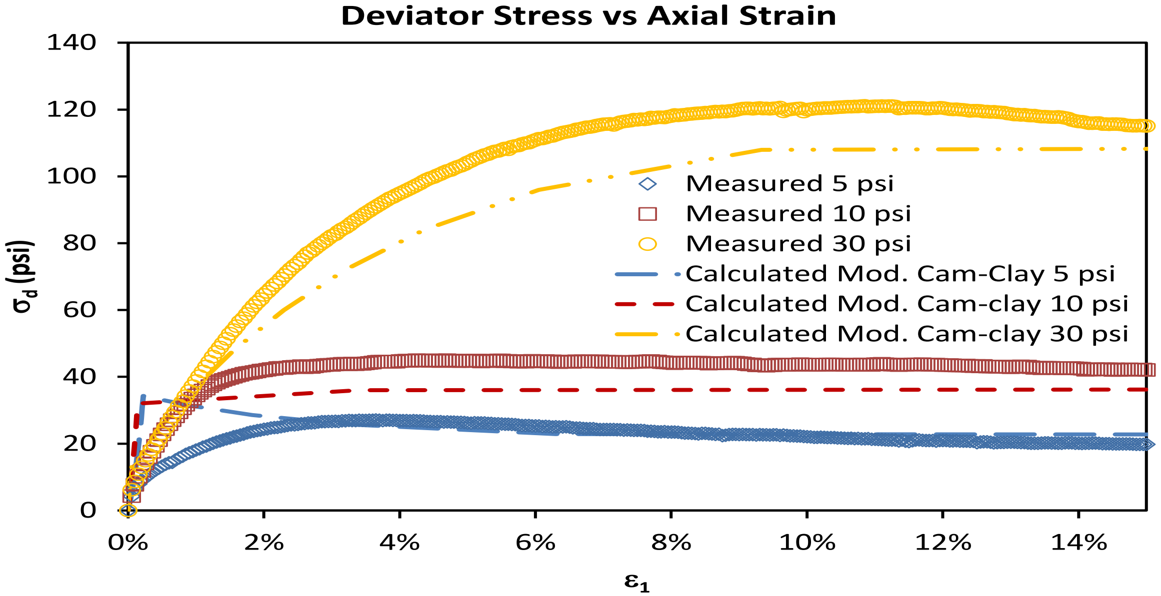

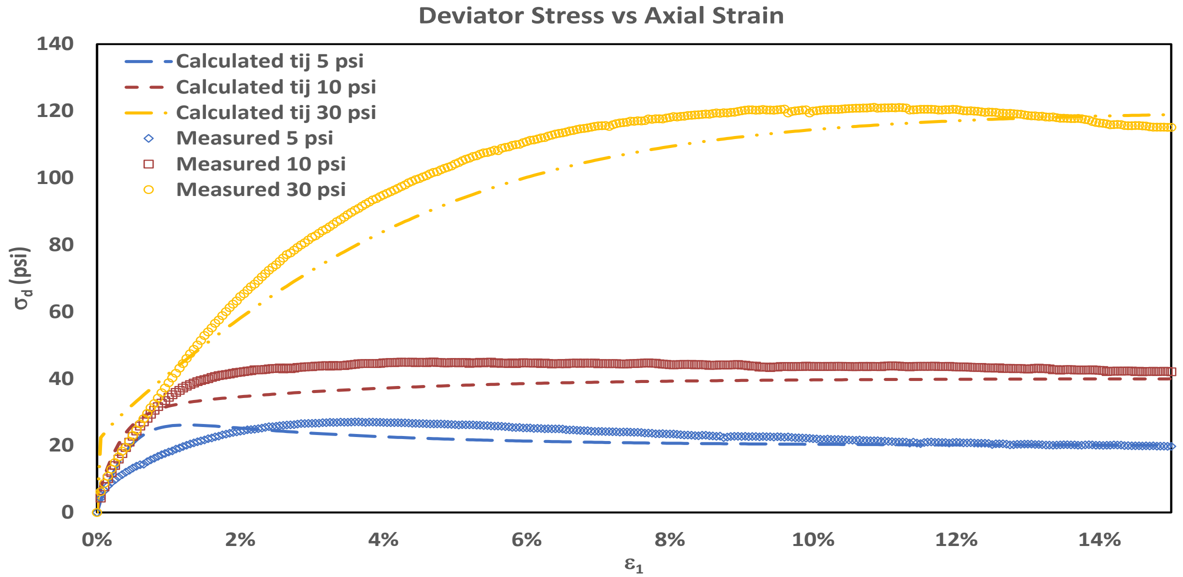

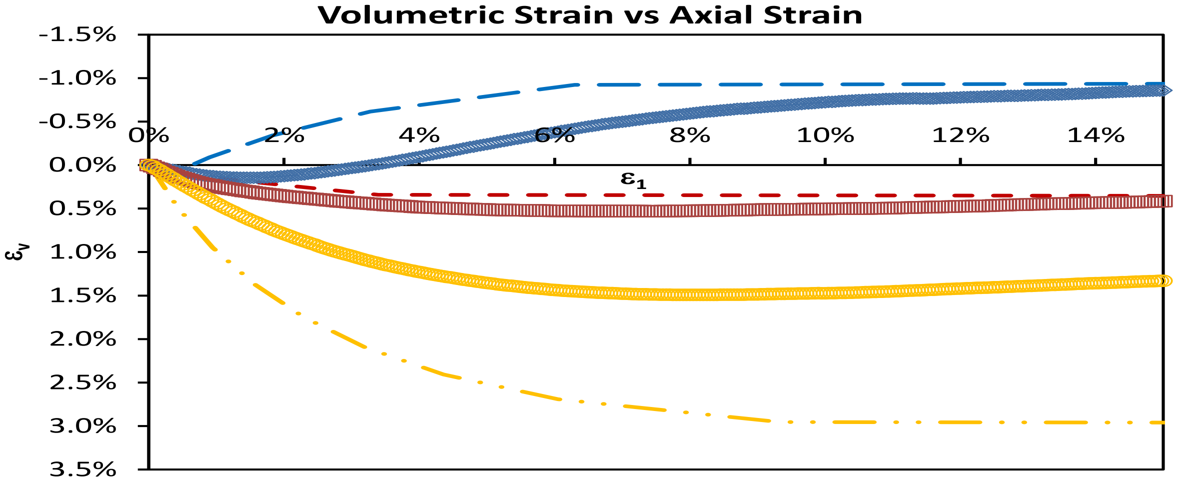

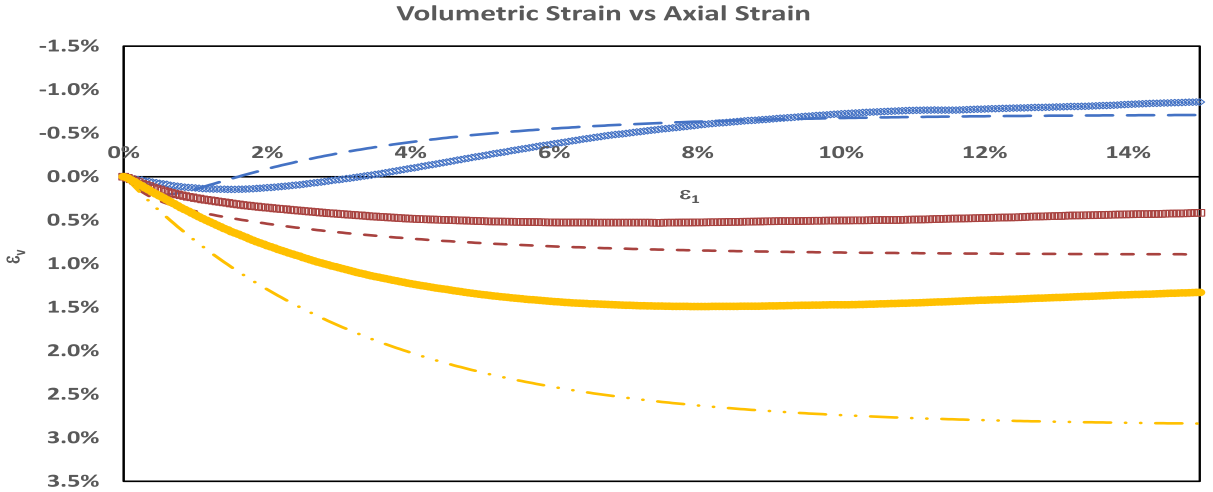

Parameter Optimization - ML

Traditional Methods (in order of Reliability):
- Analytical Derivation
- Literature Values (interface properties)
- Manual Iteration

Subloading tij Parameter Optimization:
- Subloading tij_a.exe (Para, Path, and Ana.cal files)
- Manual Iteration
- Limitations/Constraints

Potential path forward:
- Machine Learning based optimization
- Inverse Problem (Zhang et al., 2021)
- Genetic Algorithms
    - Pal et al. (1996), Samarajiva et al. (2005), and Rokonuzzaman and Sakai (2010)
- Bayesian Inference
    - Sakai and Nakano (2025), Coelho et al. (2024)

Machine Learning Framework

Bayesian Inference and Maximum-Likelihood approach

$$p(\Theta, \alpha | D) = \frac{1}{Z} p(\Theta, \alpha) p(\mathrm{D} | \Theta, \alpha)$$

Θ is the set of model parameters
α is the set of nuisance parameters
D is the set of observations
$p(\Theta, \alpha)$ is the prior distribution
$p(\mathrm{D}|\Theta, \alpha)$ is the likelihood function computed for any particular value of (Θ_i, α_i)
$Z = p(D)$ is the normalization and is independent of Θ and α

Machine Learning Framework

Markov chain Monte Carlo (MCMC) optimization for multi-variable optimization problems (Foreman-Mackey et al., 2013):

- Bayesian inference, computing and utilizing the posterior probability density function (PDF) for the model parameters
- Markov Chain - next step (set of sampling locations in the posterior probability) depends on previous set
- Monte Carlo - the approximation of the probability density functions is based on a Monte Carlo approach

Approximate posterior PDF efficiently despite parameter spaces with **high dimensionality**.
“emcee” algorithm as its **affine invariance** results in performance independent of highly anisotropic posterior PDFs (Goodman & Weare, 2010)
Basis of emcee algorithm is the **Metropolis-Hastings** (M-H) algorithm with an **affine invariant** process
Compute **N samples (steps)** $\{\Theta_i\}$ from the posterior PDF (Foreman-Mackey et al., 2013)

Machine Learning Framework

- *emcee* algorithm generates a random walk in the parameter space, $X(t_i) = [\Theta_i, \alpha_i]$ depending only on previous step $X(t_{i-1})$.
- Affine-invariance means use of a simultaneously evolving ensemble of K "walkers", $S = \{X_k\}$.
- Proposed parameter distribution for the kth walker is based on the current positions of the $K - 1$ walkers in ensemble $S[k] = \{X_j, \forall_j \neq k\}$.
- Position of walker X_k is updated by drawing random walker X_j from the ensemble $S[k]$ (Goodman & Weare, 2010).

$$
\begin{aligned}
&\text{if } r \leq q \text{ then}\\
&X_k(t+1) \leftarrow Y\\
&\text{else}\\
&X_k(t+1) \leftarrow X_k(t)\\
&\text{endif}
\end{aligned}
$$

where r is a random sample from a uniform distribution $r \sim U[0, 1]$ and Y is updated walker position

$$X_k(t) \rightarrow Y = X_j + Z\left[X_k(t) - X_j\right]$$

where Z is a random variable drawn from $g(Z = z)$.

$$g\left(z^{-1}\right) = z g(z)$$

$$g(z) \propto \begin{cases} \frac{1}{\sqrt{z}} & \text{if } z \in \left[\frac{1}{a}, a\right] \\ 0 & \text{otherwise} \end{cases}$$

where $a > 1$ (often set to 2).

Acceptance probability q:

$$q = \min\left(1, Z^{N-1} \frac{p(Y)}{p\left(X_k(t)\right)}\right)$$

Parameters from Machine Learning but….

The magnitude problem and proposed weighting schema:

1. Min-max normalization scheme:

$$\frac{1}{w_i} = 0.01 + \frac{x_i - \min(x)}{\max(x) - \min(x)}$$

2. Logarithmic weighing scheme:

$$w_i = \begin{cases} \dfrac{1}{\log x_i} & for\ x_i \geq 1 \\ \dfrac{1}{|\log(1000 * x_i)|} & for\ x_i \leq 1 \end{cases}$$

3. Reverse Sequential weighing scheme:

$$w_i = \frac{i}{\mathrm{count}(x)} * \left(\max(x) - \min(x)\right)$$

Parameters from Machine Learning

Parameter	Value	Description
N	0.3576	Void ratio at reference pressure (1 atm)
λ	0.0207	Virgin compression index (slope of NC line)
β	1.0515	Yield function shape parameter
a	103.32	Density function parameter
k_a	1.0	Shear control parameter for density function
R_{cs}	5.0852	Principal stress ratio at critical state in triaxial compression

Additional Outputs:
χ^2
Reduced χ^2
Akaike and Bayesian Info Criteria
R^2
Parameter CI and Standard Error
Parameter Correlation

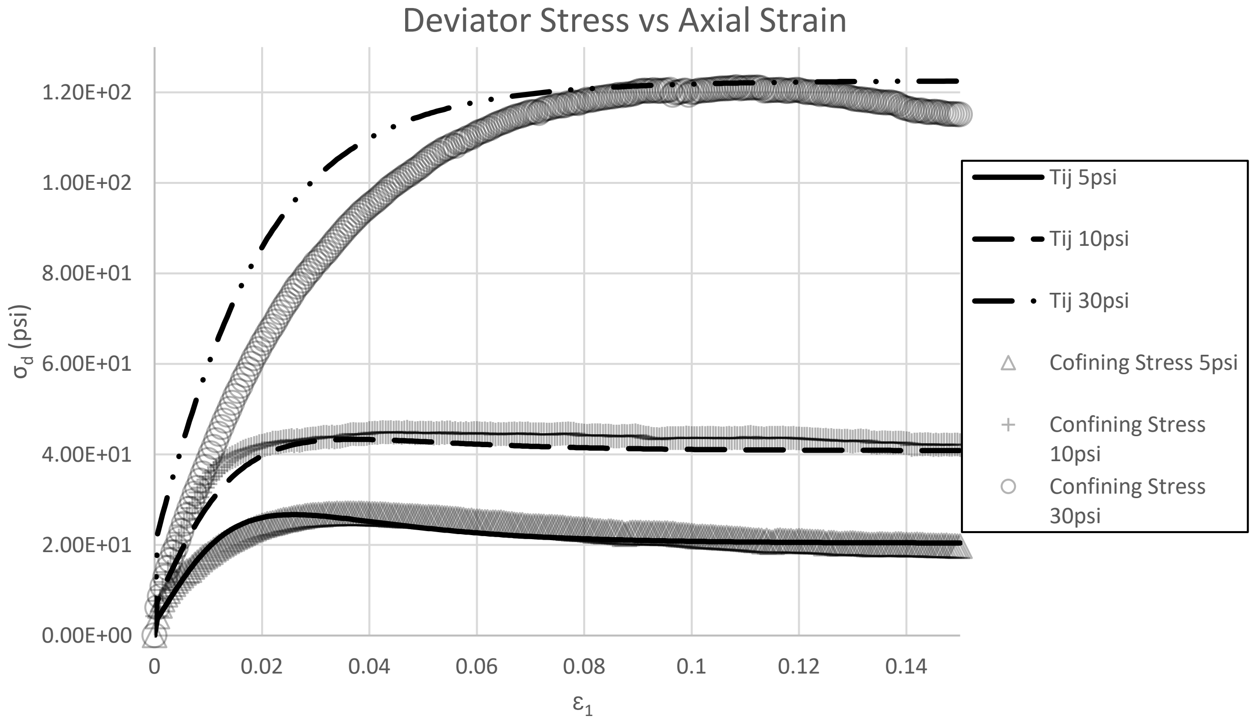

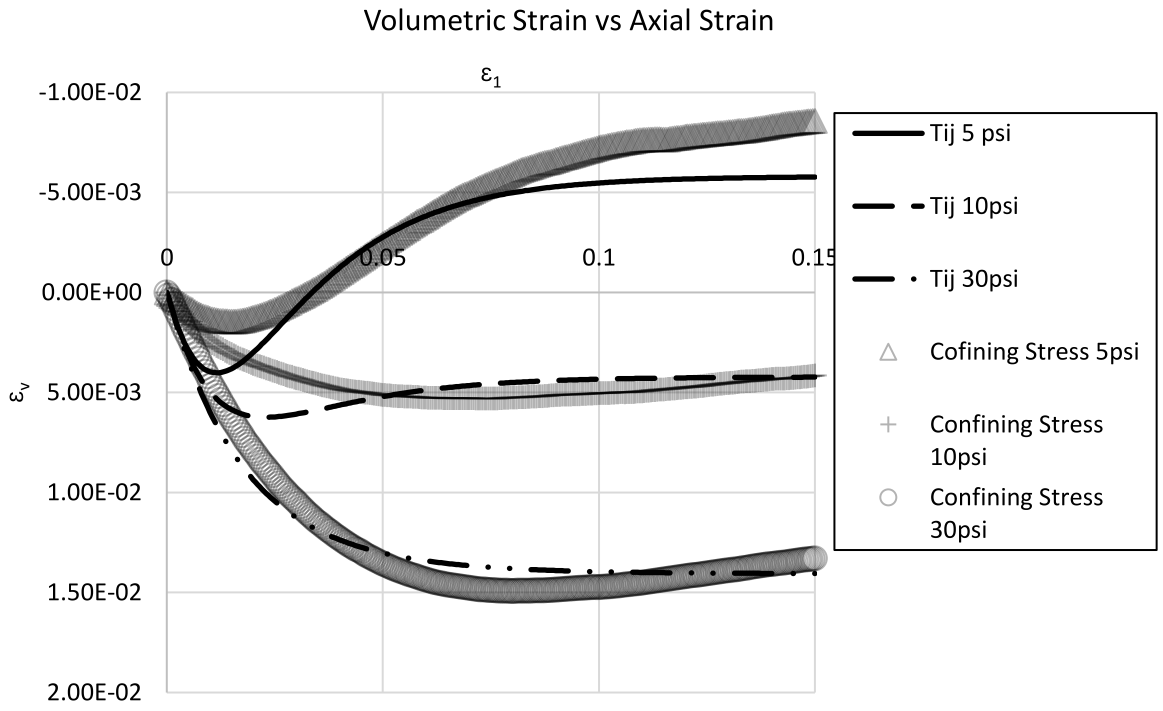

Parameters from Machine Learning but….

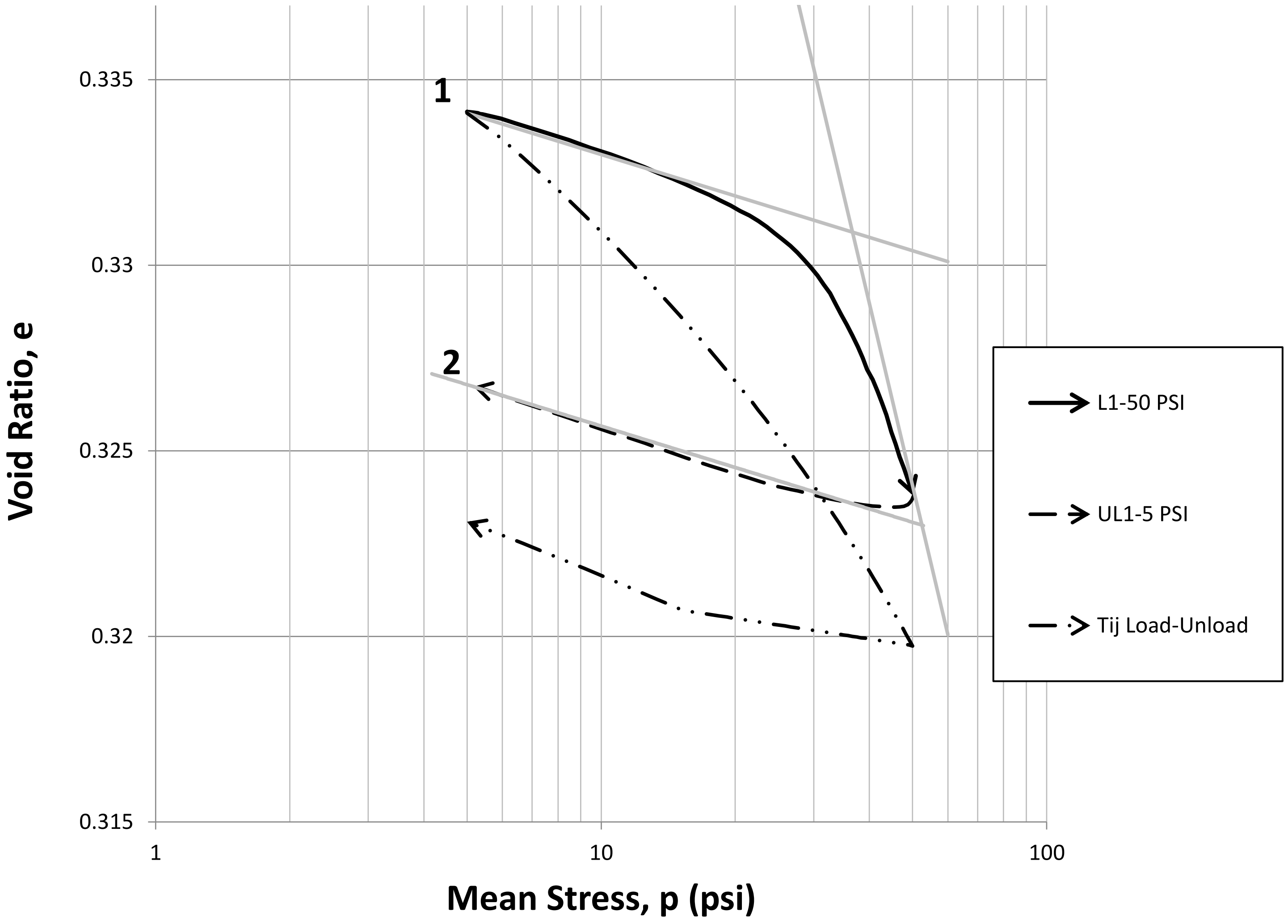

Parameter Results

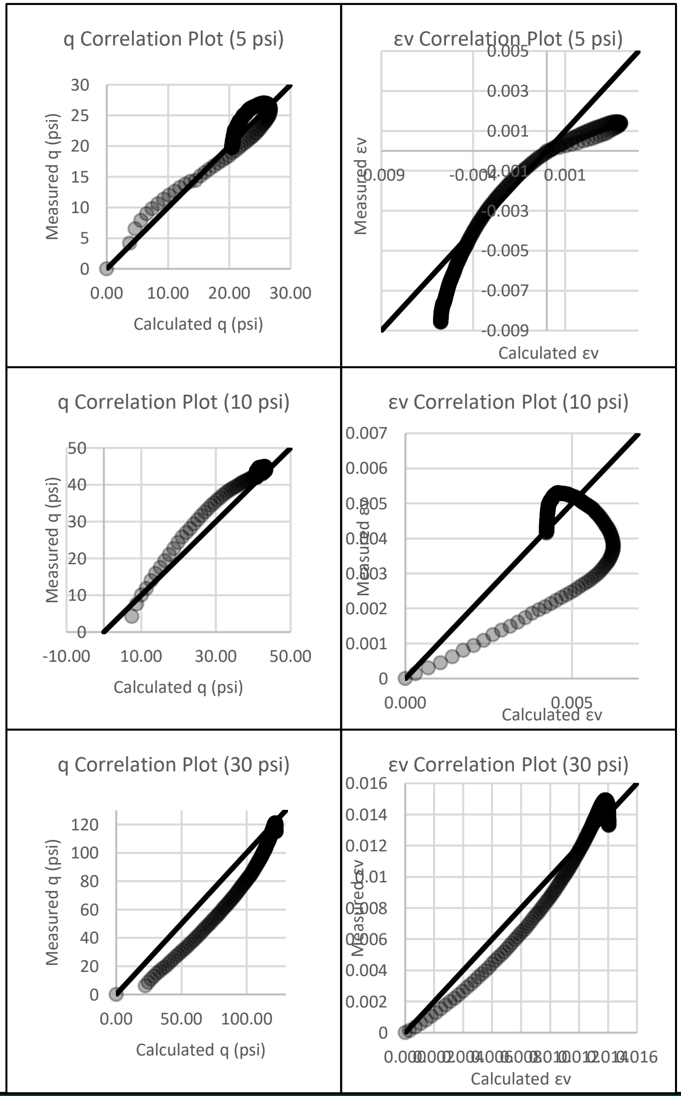

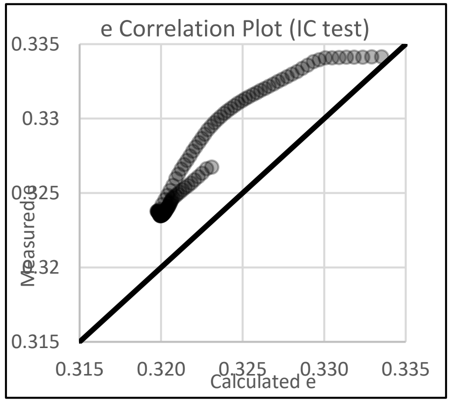

Metric	R^2	R	CoV	SRS	C_v	SRS/CoV
q (σ_3 = 5 psi)	0.87149	0.93353	13.2681	776.467	0.16267	58.5215
q (σ_3 = 10 psi)	0.97273	0.98627	41.5877	1930.47	0.15394	46.4191
q (σ_3 = 30 psi)	0.96990	0.98483	667.609	37600.4	0.25723	56.3210
ε_v (σ_3 = 5 psi)	0.91773	0.95798	1.12E-05	8.19E-04	-0.77546	73.1438
ε_v (σ_3 = 10 psi)	0.11306	0.33625	3.22E-05	67.7767	1.26982	2104572
ε_v (σ_3 = 30 psi)	0.96699	0.98335	1.09E-05	2.26E-04	0.26772	20.6589
e	0.90187	0.94967	1.32E-05	0.10652	0.01109	8082.67
Average	0.82695	0.88519				
Average (w/o ε_v [σ_3 = 10 psi])	0.92894	0.96362				

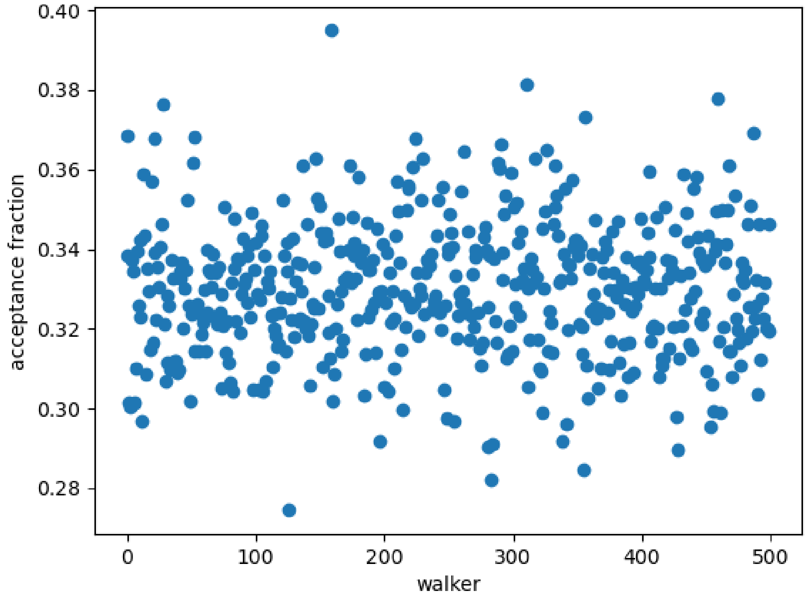

Parameter Results

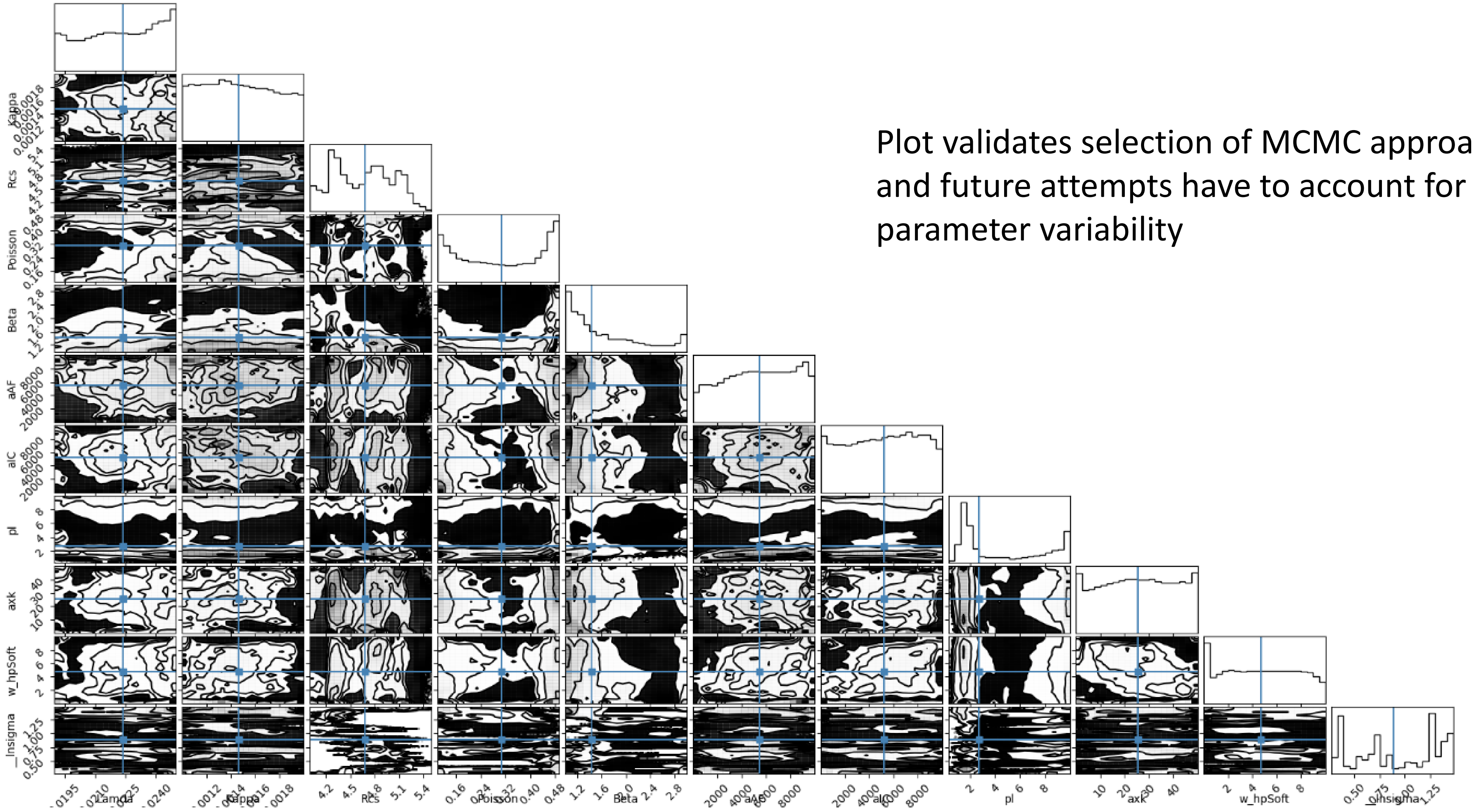

Plot validates selection of MCMC approach and future attempts have to account for modal parameter variability

Parameters from Machine Learning

Parameter	Value	Description
N	0.3576	Void ratio at reference pressure (1 atm)
λ	0.0207	Virgin compression index (slope of NC line)
β	1.0515	Yield function shape parameter
a	103.32	Density function parameter
k_a	1.0	Shear control parameter for density function
R_{cs}	5.0852	Principal stress ratio at critical state in triaxial compression

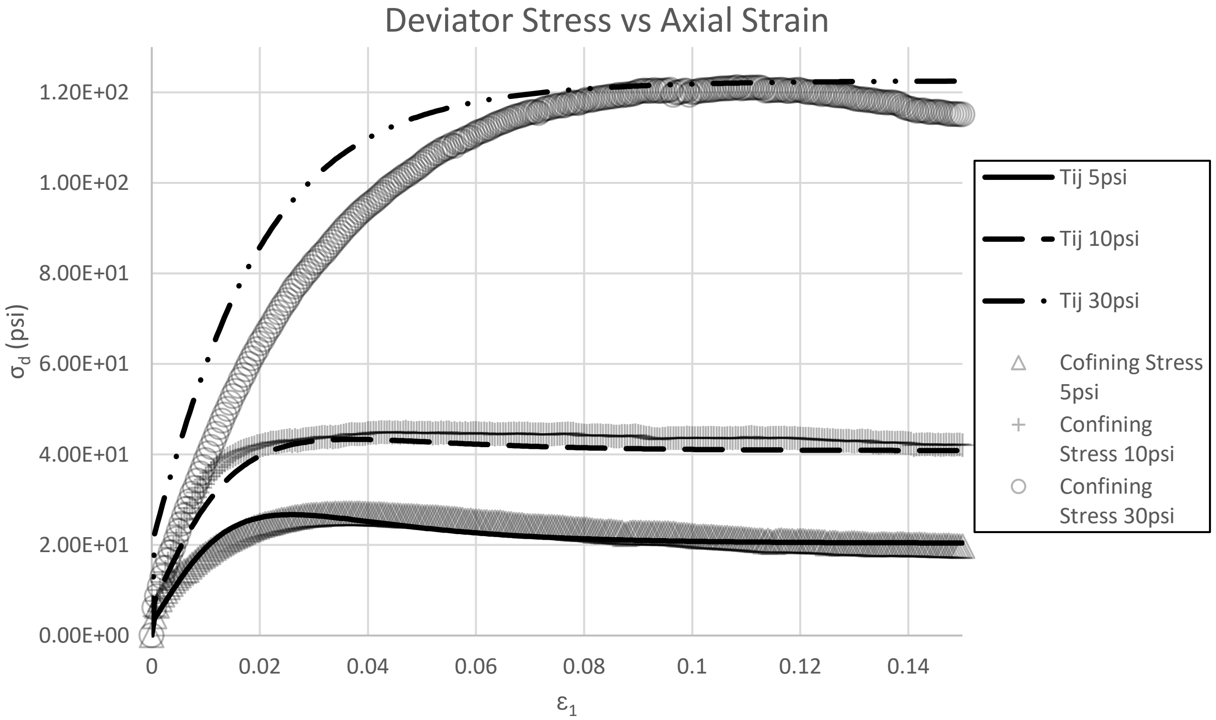

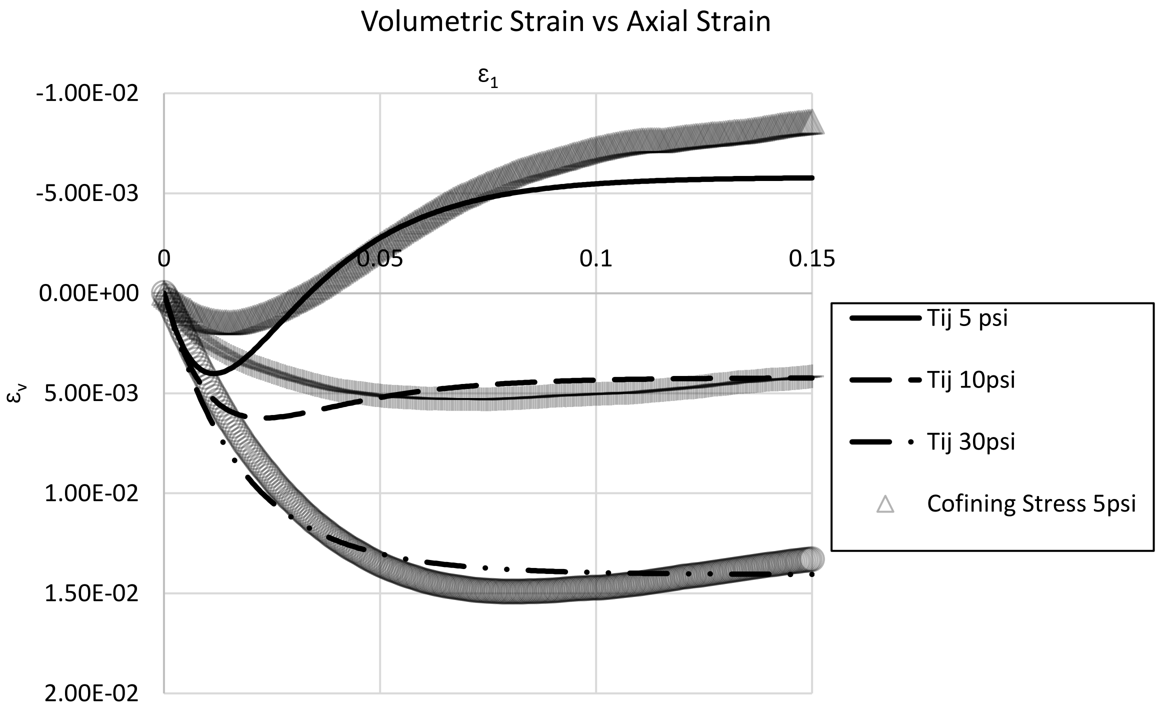

Parameters from Machine Learning but….

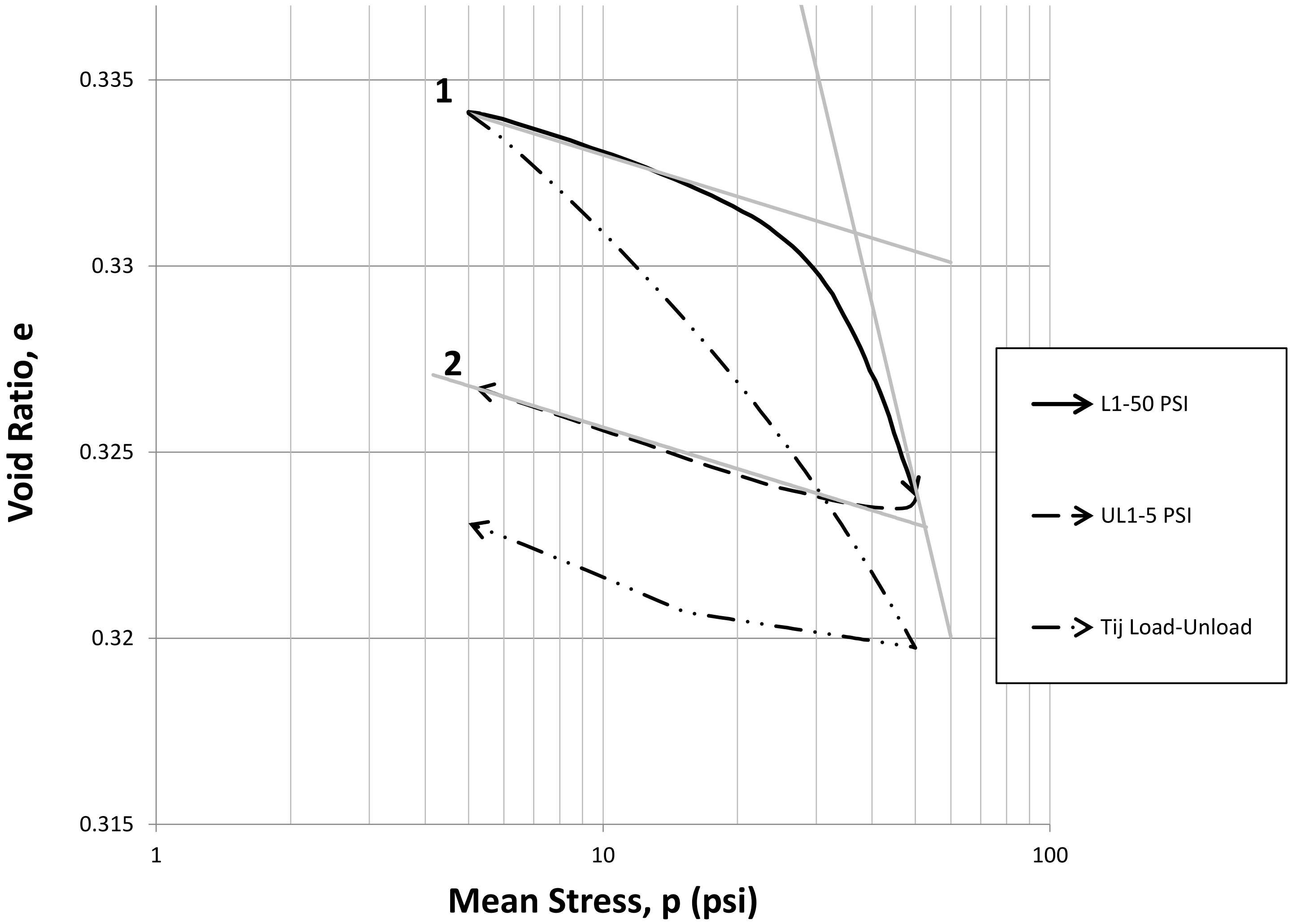

Geotextile Parameters

Test	Geotextile Manufacturer	Wide Width Tensile Strength (lb/ft)	Wide width tensile strength at 5% strain (lb/ft)	Tensile Strength (Grab) (lb)	Wide Width Elongation (%)
TF-6, -7, TF-9, -10	Propex	4800 x 4800	660 x 1500	600 x 500	(10 x 8%)

- Biaxial, woven polypropylene Propex Geotex 4X4HF geotextile
- Ideally want geotextile strength to decay after yield
- Geotextile modeled as biaxial, bilinear elastoplastic

Geotextiles		
Parameter	**Value**	**Unit**
EA_1	876	kN/m
EA_2	701	kN/m
Tf	70.05	kN/m

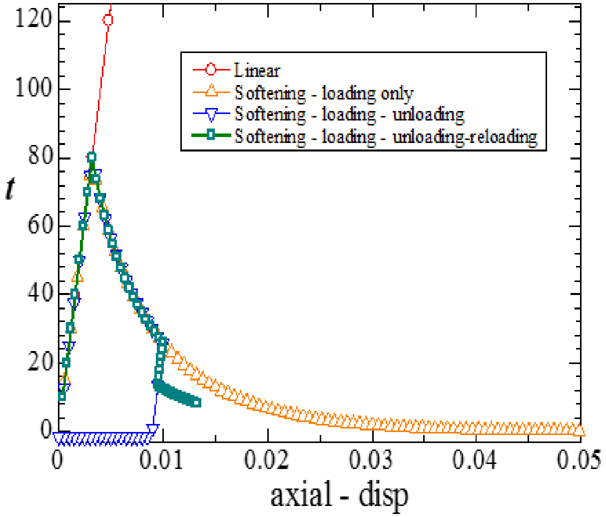

Geotextile wide width tensile force vs axial strain

Interface Elements

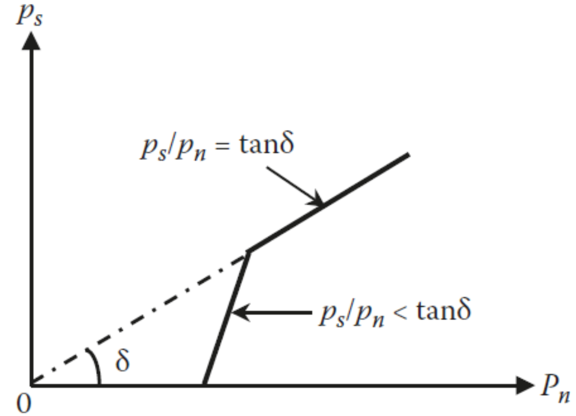

(a) Relation between normal stress (p_n) and shear stress (p_s)

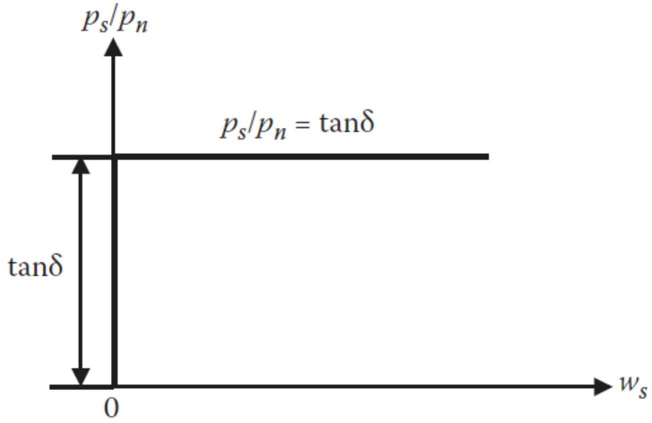

(b) Relation between relative displacement (w_s) and stress ratio (p_s/p_n)

Idealized interface behavior (Nakai T. , 2013)

Idealized interface behavior (Nakai T. , 2013)

Interface (Geotextile-Soil)		
Parameter	**Value**	**Unit**
k_n	$100.0 * 10^6$	kN/m^3
k_s	$9.09 * 10^6$	kN/m^3
ν	0	-
ϕ	40	°
ψ	0	°
c_{ref}	0	kPa
Interface (Footing-Soil)		
Parameter	**Value**	**Unit**
k_n	$100.0 * 10^6$	kN/m^3
k_s	$9.09 * 10^6$	kN/m^3
ν	0	-
ϕ	44	°
ψ	0	°
c_{ref}	0	kPa

Geo-Research Institute (2022)

Modelling of TF10 and TF7

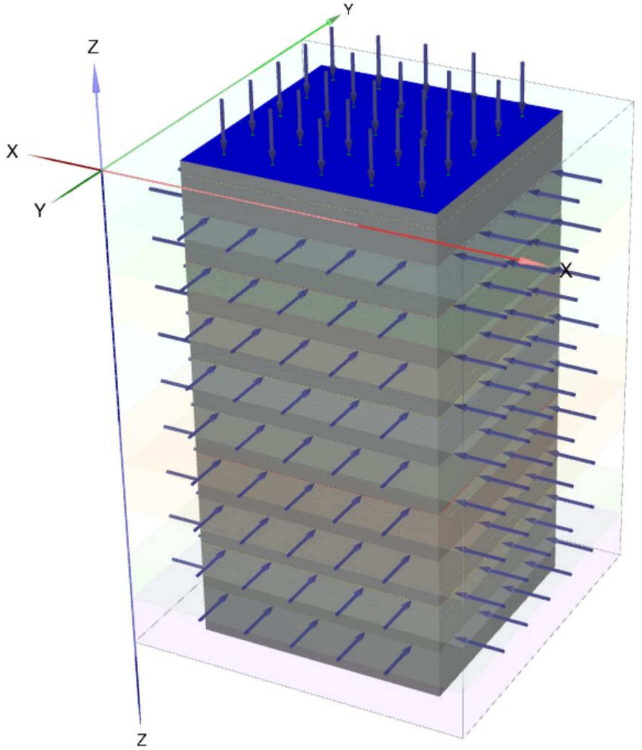

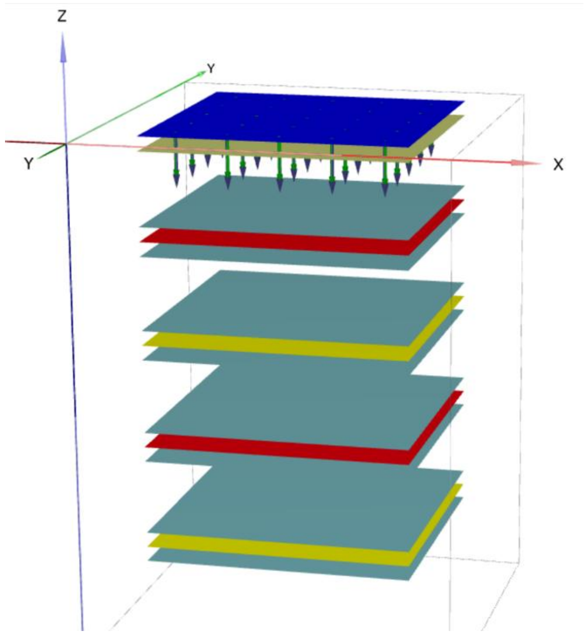

TF10

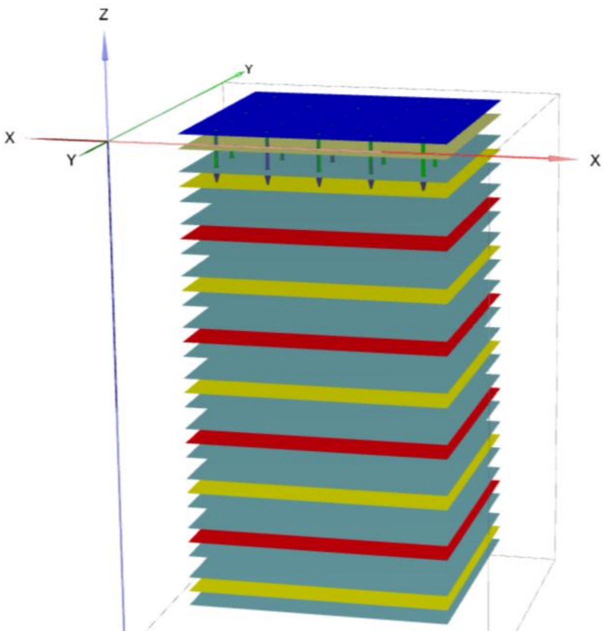

TF7

Modelling of TF10

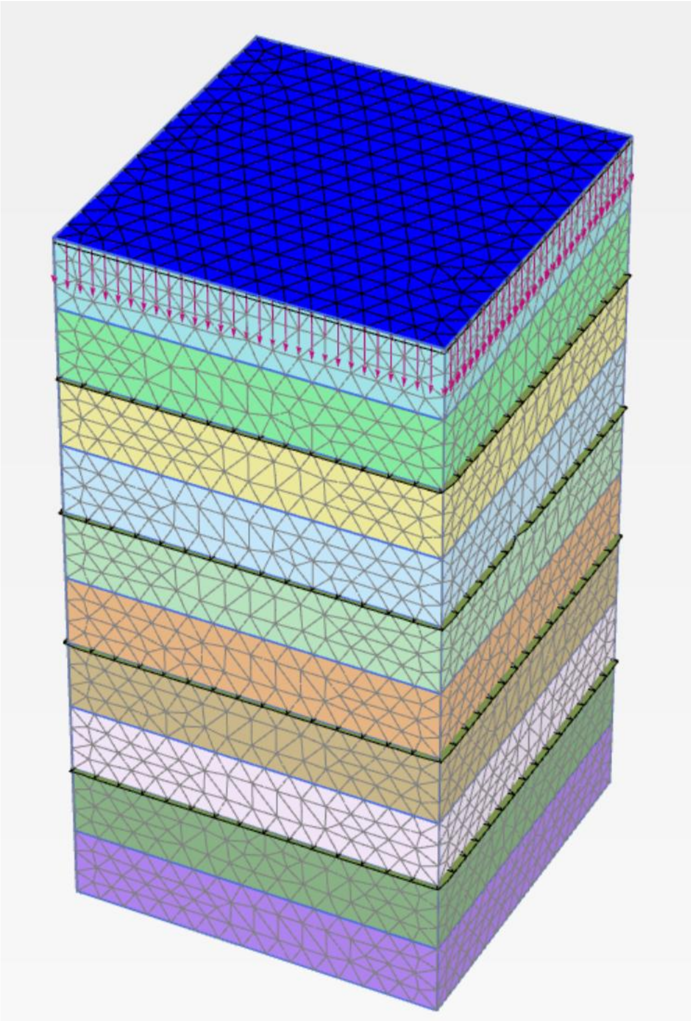

Name	Value
General	
ID	Phase_1
Start from phase	Initial phase
Calculation type	Plastic
Loading type	Staged construction
ΣM_{stage}	1.000
ΣM_{weight}	1.000
Pore pressure calculation type	Phreatic
Time interval	0.000 day
First step	1
Last step	100
Special option	0
Deformation control parameters	
Ignore undr. behaviour (A,B)	☐
Reset displacements to zero	☑
Reset small strain	☑
Reset state variables	☐
Reset time	☐
Updated mesh	☐
Ignore suction	☑
Cavitation cut-off	☐
Cavitation stress	100.0 kN/m²
Numerical control parameters	
Solver type	Pardiso (multicore direct)
Max cores to use	256
Max number of steps stored	1
Use compression for result files	☐
Use default iter parameters	☐
Max steps	1000
Tolerated error	0.5000
Max unloading steps	5
Max load fraction per step	0.01000
Over-relaxation factor	1.200
Max number of iterations	60
Desired min number of iterations	6
Desired max number of iterations	15
Arc-length control type	Auto
Use subspace accelerator	☐
Subspace size	3
Use line search	☑
Use gradual error reduction	☐

Soil - User-defined - GW1

General | Mechanical | Groundwater | Interfaces | Initial

Property	Unit	Value
User-defined model		
DLL file		tij120plaxis_3dexp64.dll
Model in DLL		NoTension/Subloading tij AF
User-defined parameters		
λ		0.03250
κ		1.600E-3
R_{cs}		5.000
N (void ratio under atmospheric pressure)		0.3640
ν (Poisson ratio)		0.2000
Beta (Shape of yeild surf. Beta>1.0 is recommended)		1.155
e_0 (void ratio under initial stress)		0.2450
[Density] a		400.0
[Density] k_a		10.00
[Bonding] Q_{c0}		0.000
[Bonding] b		0.000
[Bonding] k_b		0.000
[Unit] Pa (Atmospheric pressure) [Be careful of what unit system you use]	kN/m²	100.0
[IC component] wgtIC		1.000
[IC component] powerIC		2.000
[Advanced] SplitStrainFlag (You should let it be 0.0.)		0.000
[Advanced][e_0] e_{0inc}		0.000
[Advanced][e_0] Z_{ref}	m	0.000
[Advanced][e_{max}] e_{max}		0.5510

Next | OK | Cancel

Load-settlement

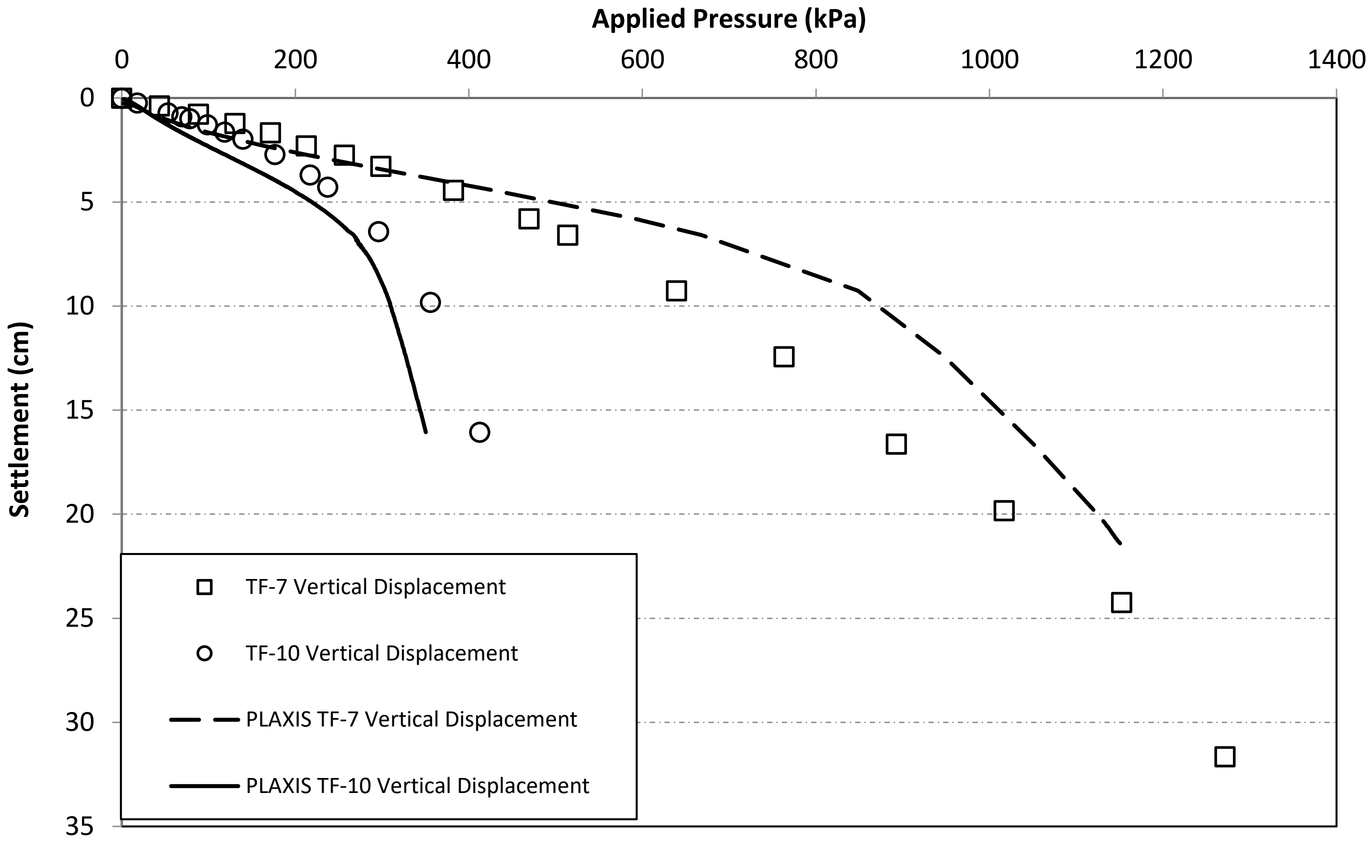

GRS Pier	R^2	R	CoV	SRS	C_v	SRS/CoV
TF - 7	0.96413	0.98190	150905	1.73E+05	0.883934	1.145405
TF - 10	0.99046	0.99522	16753	3.72E+04	0.720752	2.22
Average	0.97730	0.98856				

Lateral Deformation TF7

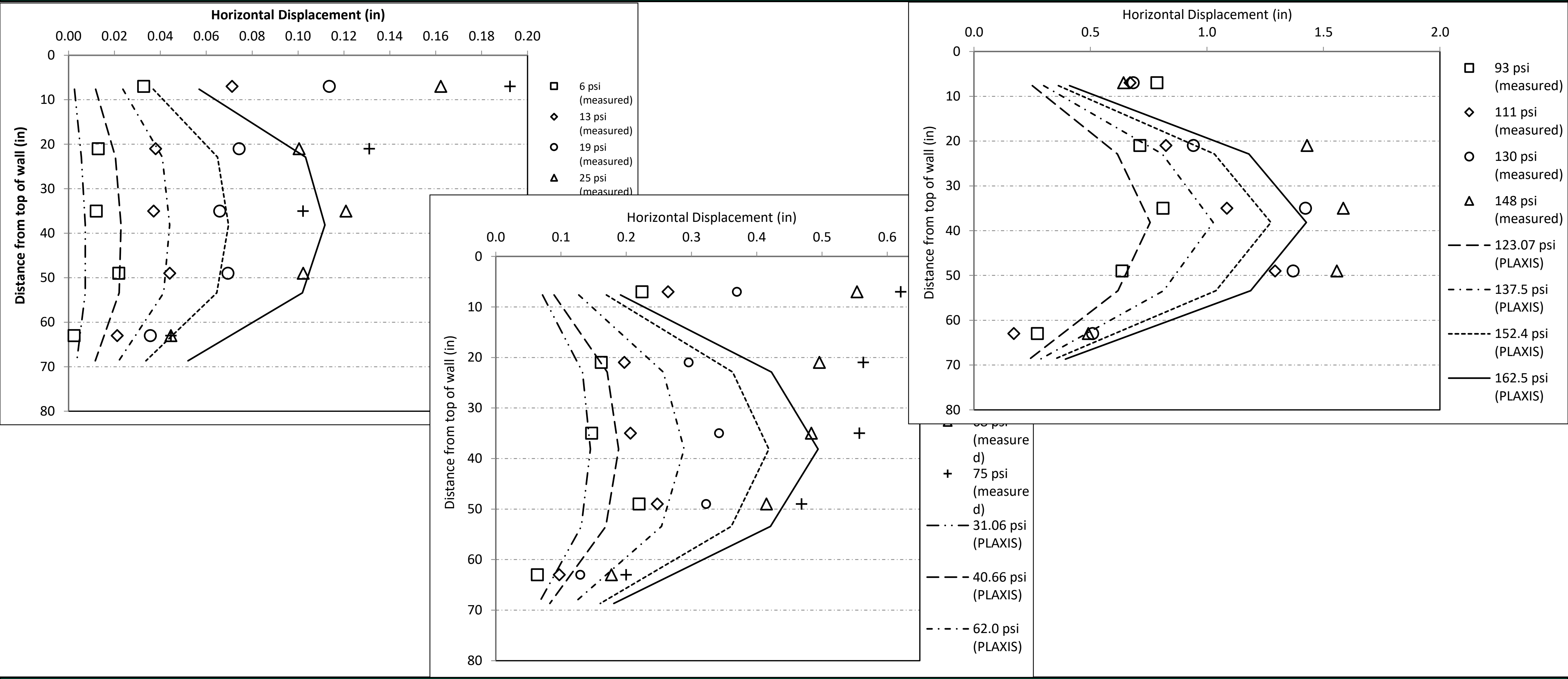

Lateral Deformation TF10

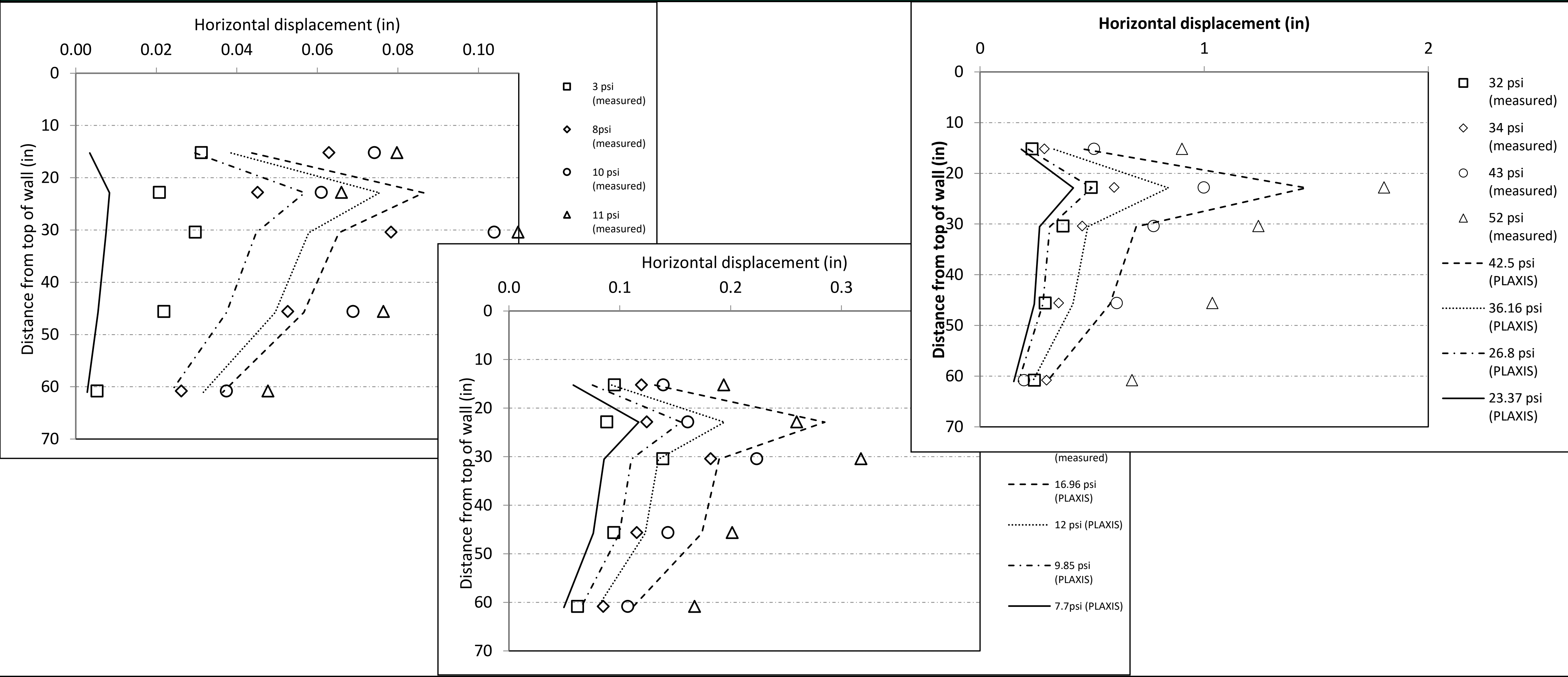

Geotextile Force Distribution in TF7

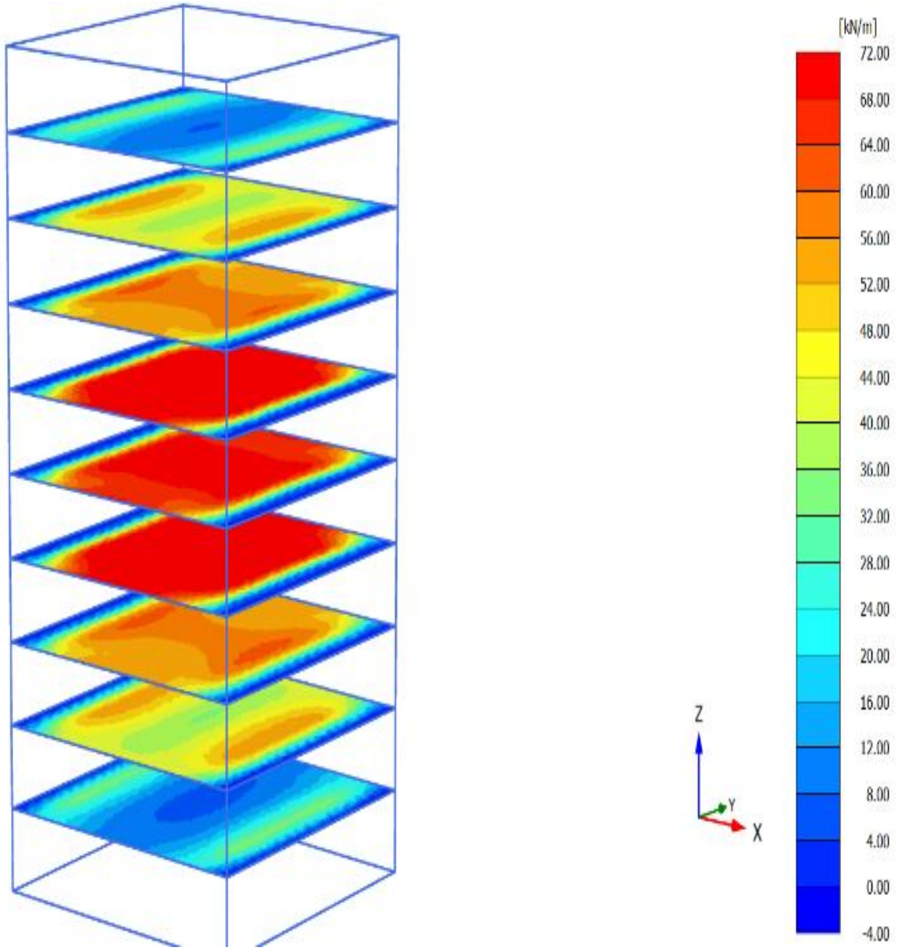

N_1 (in-plane force, kN/m)

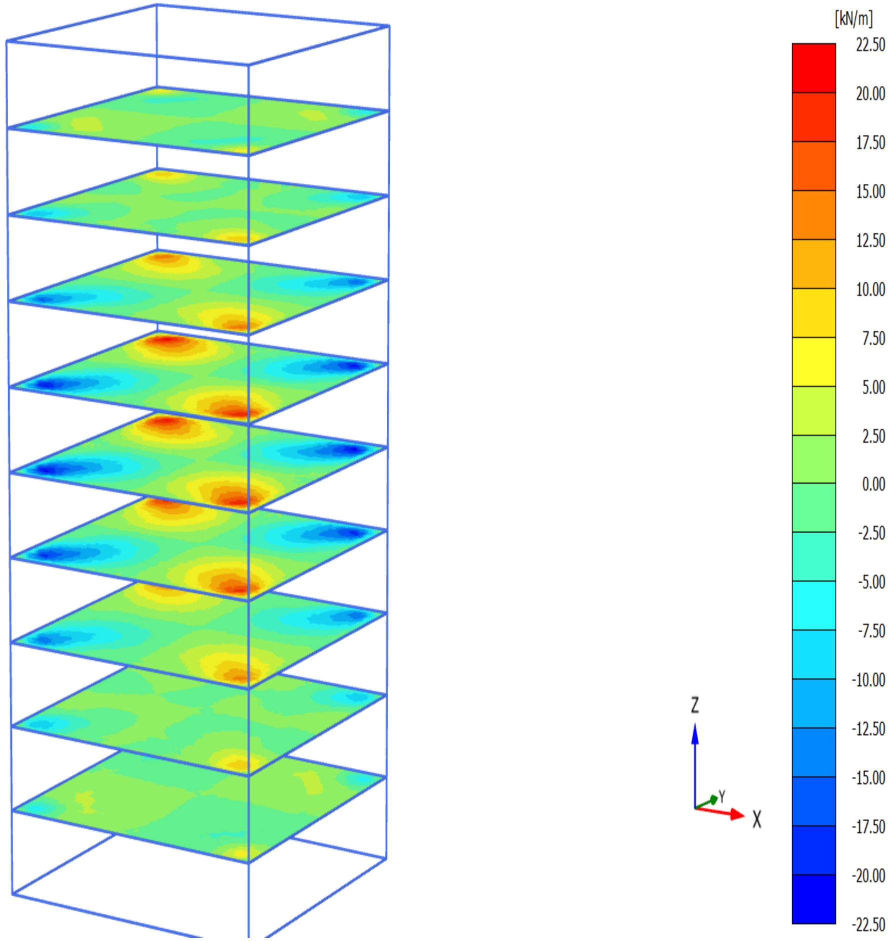

Q_{12} (in-plane shear, kN/m) - Right

Deviatoric Strain, γ_s, Distribution in TF7

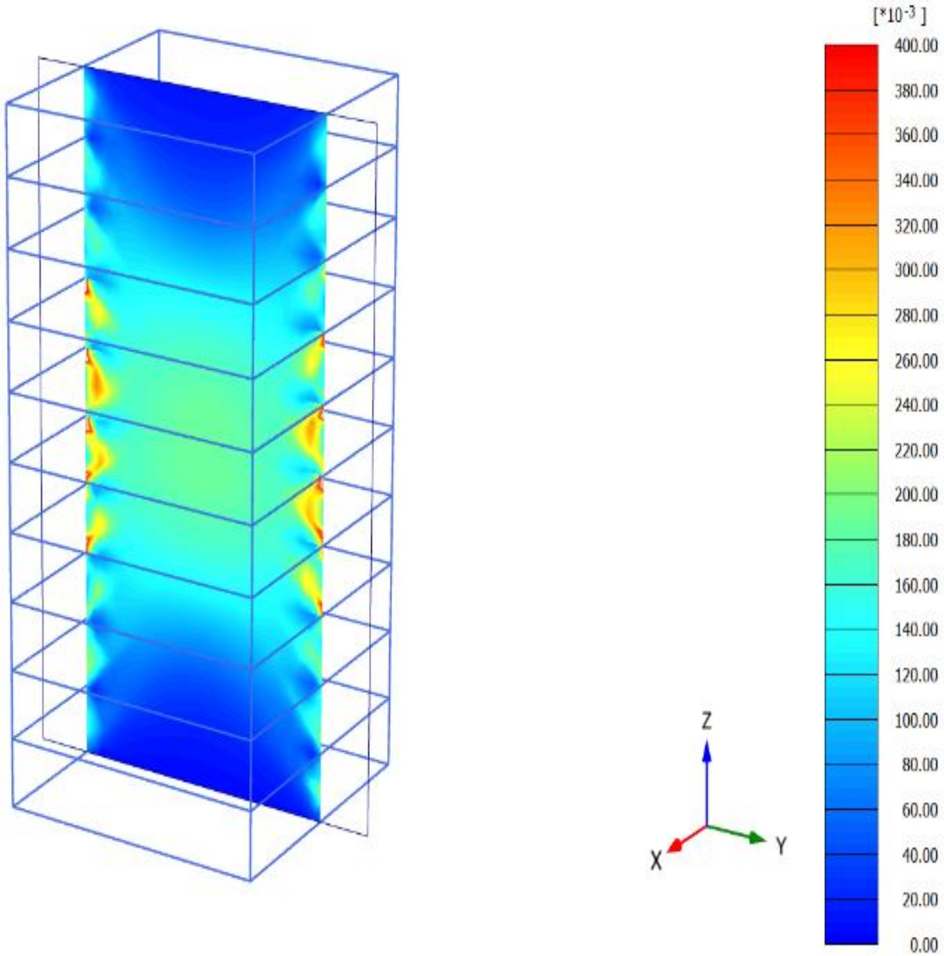

YZ cross-section

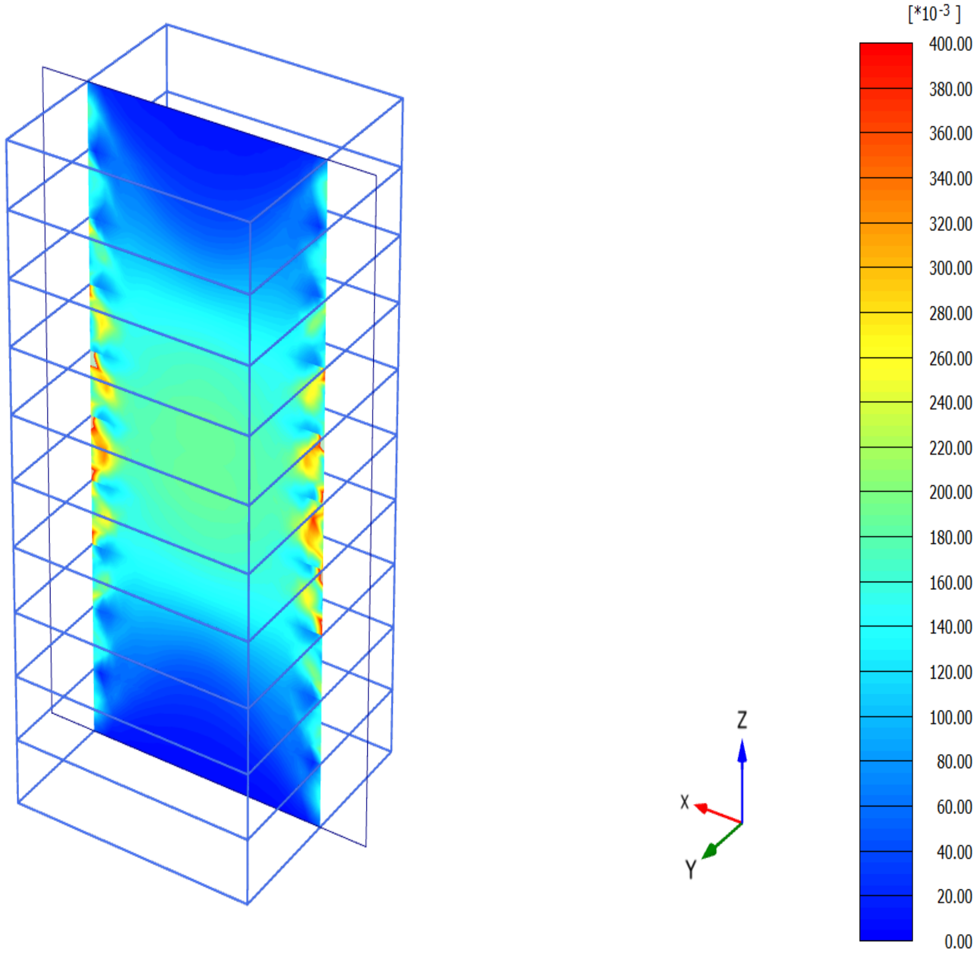

XZ cross-section

Geotextile Force Distribution in TF10

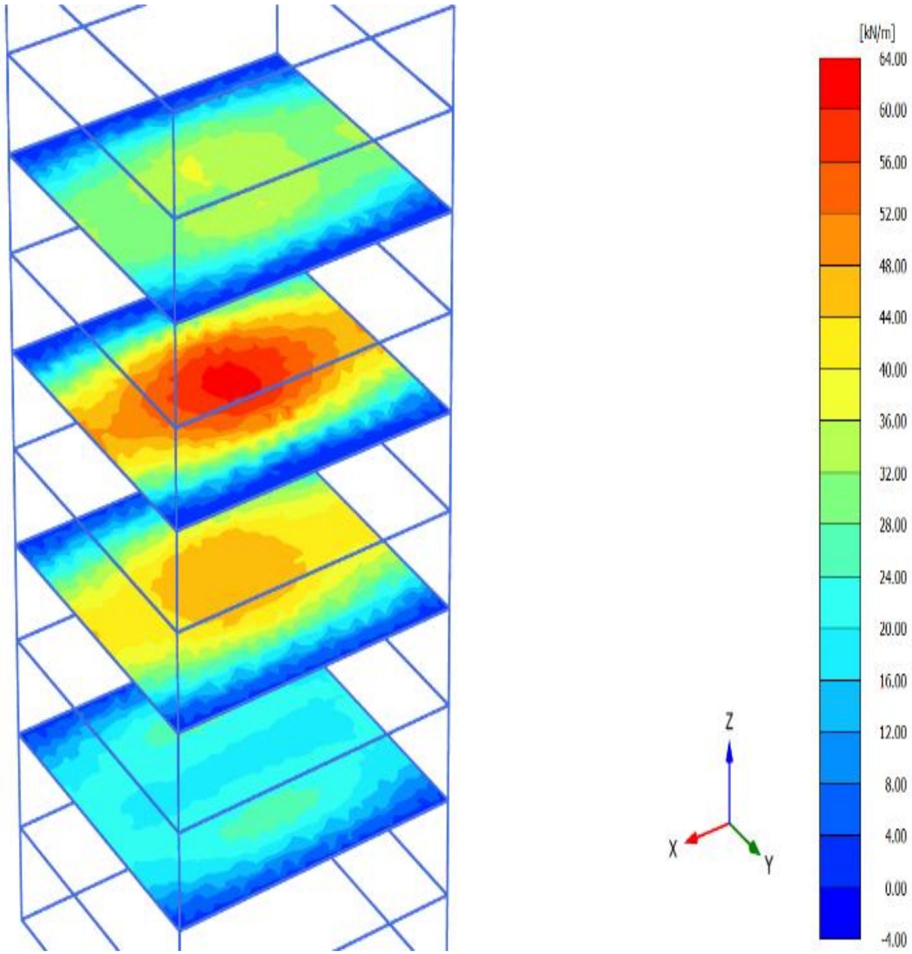

N_1 (in-plane force, kN/m)

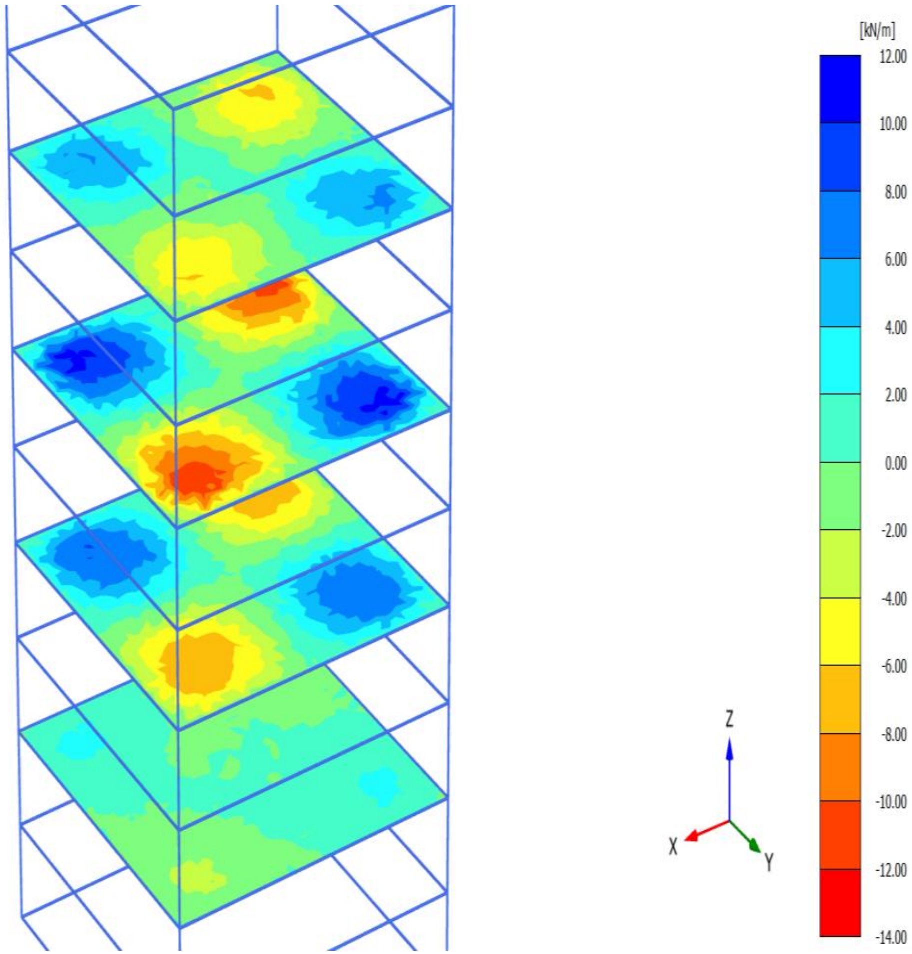

Q_{12} (in-plane shear, kN/m) - Right

Deviatoric Strain, γ_s, Distribution in TF10

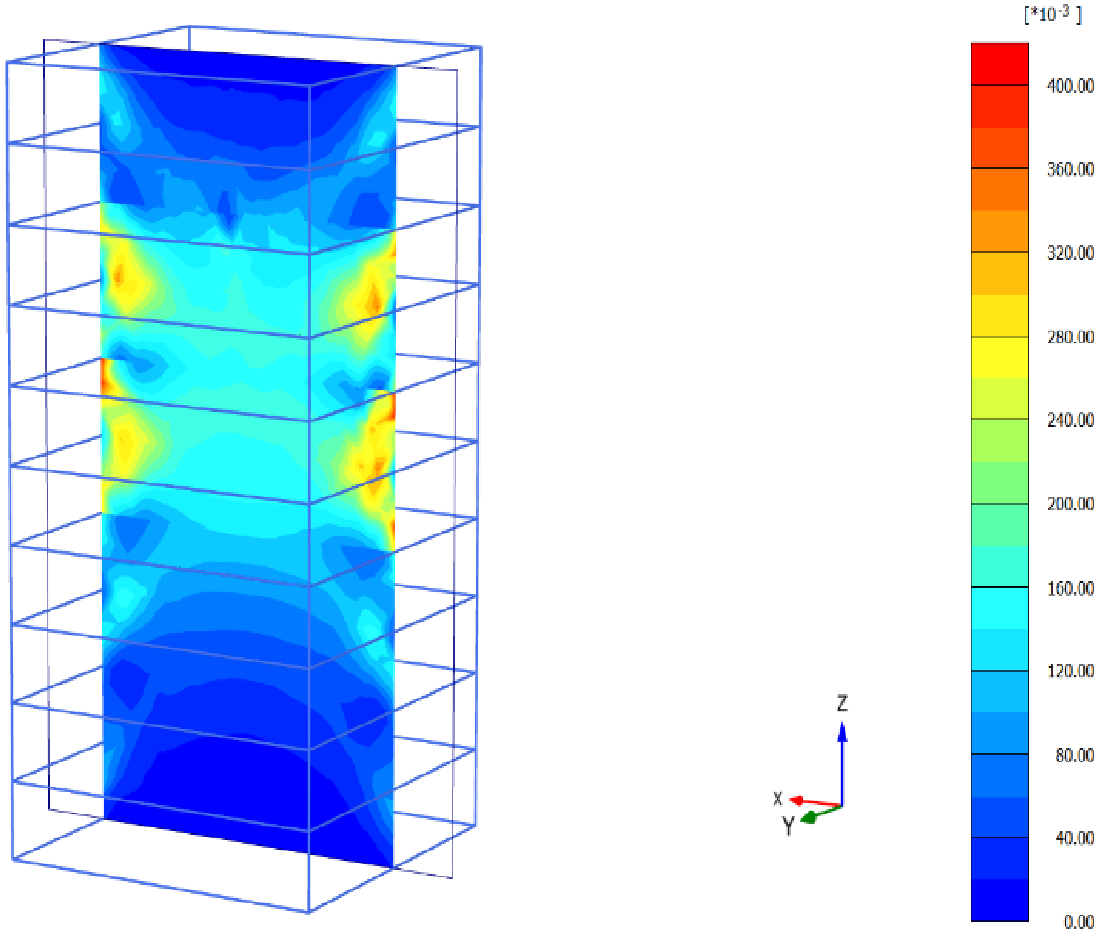

XZ cross-section

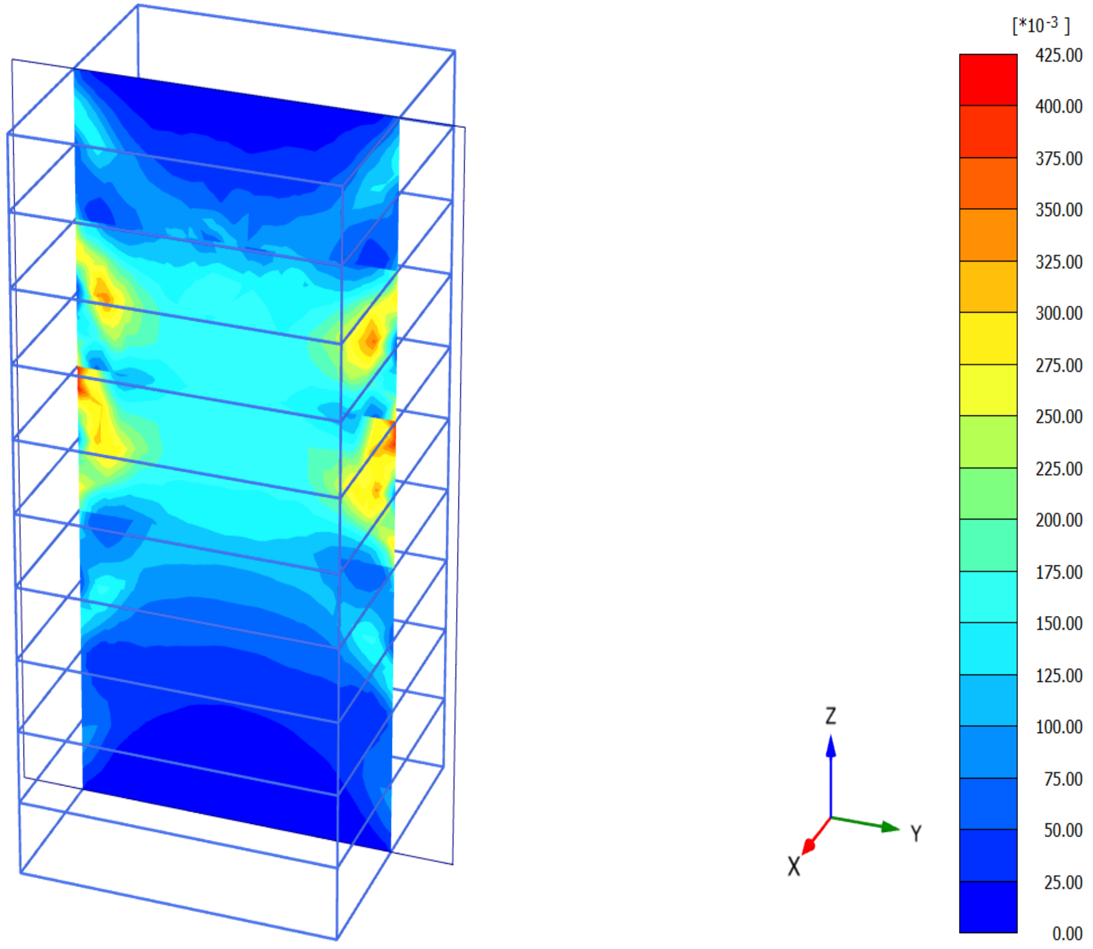

YZ cross-section

Summary and Conclusions

- Using machine learning, optimization of parameters should be performed for both triaxial compression and consolidation tests with appropriate weighting for each
- Combined FEM with DEM may be necessary to consider spalling of soil in unfaced GRS columns
- Beginnings of shear planes can be seen in deviatoric strain plots despite use of associated plasticity in Subloading t_{ij} model
- Stress development primarily occurred in the central geotextile reinforcement layers

Summary and Conclusions

- Using machine learning, optimization of parameters should be performed for both triaxial compression and consolidation tests with appropriate weighting for each
- Combined FEM with other methods (MPM/SPH/DEM?) may be necessary to consider spalling of soil in unfaced GRS columns
- Beginnings of shear planes can be seen in deviatoric strain plots despite use of associated plasticity in Subloading t_{ij} model
- Stress development primarily occurred in the central geotextile reinforcement layers

Load Testing

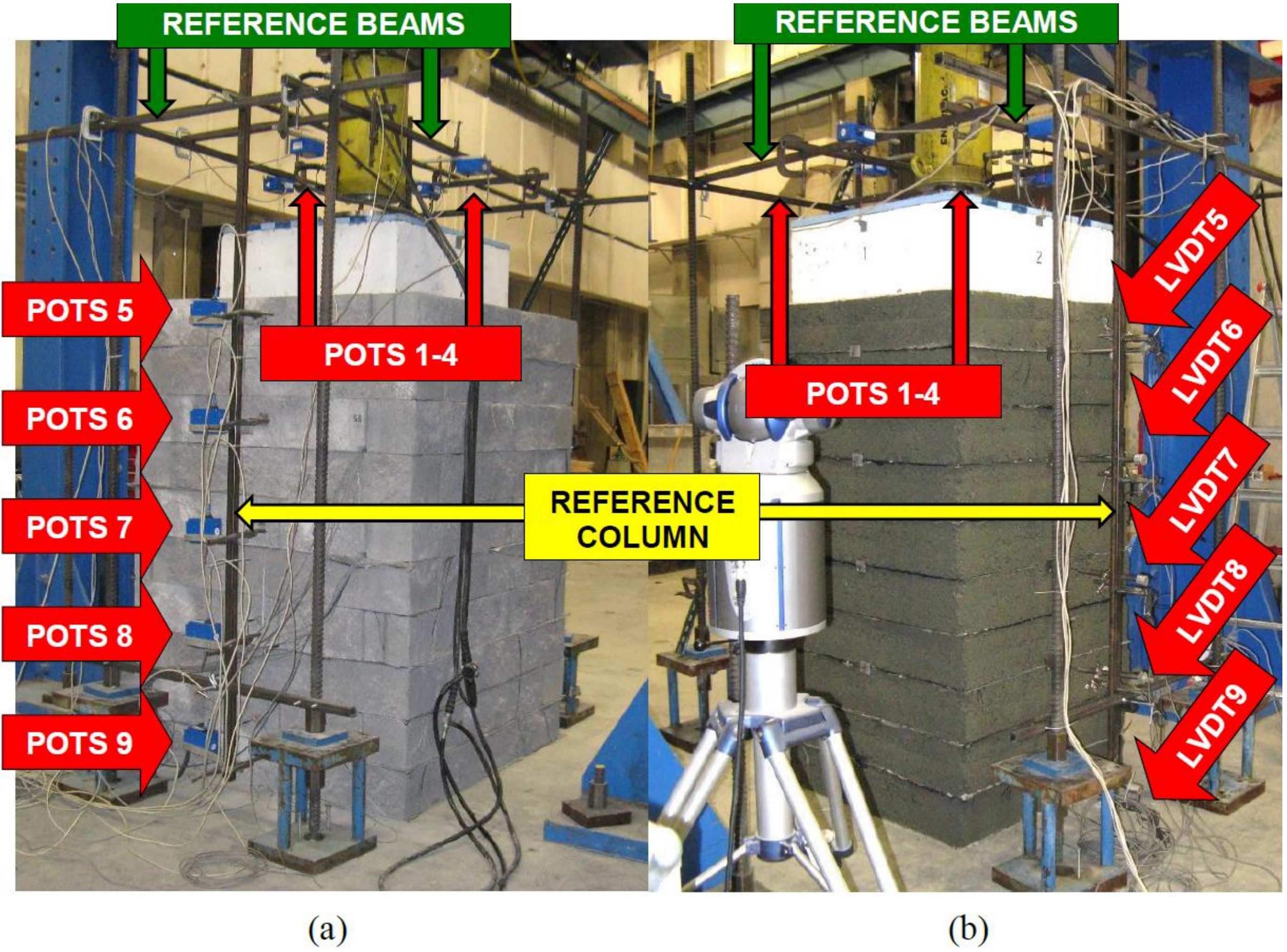

Schematics of deflection instrumentation for mini piers (a) with facing and (b) without facing. (Iwamoto, 2014)

TF-10 at failure with S_v = 15¼ inches, T_f = 4,800 lb/ft, and VDOT 21A material. (Nicks et al., 2013)

Summary and Conclusions

- Using machine learning, optimization of parameters should be performed for both triaxial compression and consolidation tests with appropriate weighting for each
- Combined FEM with other methods (MPM/SPH/DEM?) may be necessary to consider spalling of soil in unfaced GRS columns
- Beginnings of shear planes can be seen in deviatoric strain plots despite use of associated plasticity in Subloading t_{ij} model
- Stress development primarily occurred in the central geotextile reinforcement layers

Summary and Conclusions

- Using machine learning, optimization of parameters should be performed for both triaxial compression and consolidation tests with appropriate weighting for each
- Combined FEM with other methods (MPM/SPH/DEM?) may be necessary to consider spalling of soil in unfaced GRS columns
- Beginnings of shear planes can be seen in deviatoric strain plots despite use of associated plasticity in Subloading t_{ij} model
- Stress development primarily occurred in the central geotextile reinforcement layers

References

- Adams, M., Nicks, J., Stabile, T., Wu, J., Schlatter, W., & Hartmann, J. (2011, January). Geosynthetic Reinforced Soil Integrated Bridge System Synthesis Report. Geosynthetic Reinforced Soil Integrated Bridge System Synthesis Report. Federal Highway Administration. Retrieved from https://www.fhwa.dot.gov/publications/research/infrastructure/structures/11027/index.cfm
- Foreman-Mackey, D., Hogg, D. W., Lang, D., & Goodman, J. (2013, March). emcee: The MCMC Hammer. Publications of the Astronomical Society of the Pacific, 125, 306-312. doi:10.1086/670067
- Goodman, J., & Weare, J. (2010, January). Ensemble samplers with affine invariance. Communications in Applied Mathematics and Computational Science, 5, 65-80. doi:10.2140/camcos.2010.5.65
- Hashiguchi, K. (1989). Subloading surface model in unconventional plasticity. International Journal of Solids and Structures, 25, 917-945. doi:10.1016/0020-7683(89)90038-3
- Geo Institute (2019). Shear and Normal Stiffness of Interface Elements when Using Subloading tij. Shear and Normal Stiffness of Interface Elements when Using Subloading tij.
- Iwamoto, M. K. (2014, May). Observations from Load Tests on Geosynthetic Reinforced Soil. Ph.D. dissertation. Retrieved from https://scholarspace.manoa.hawaii.edu/items/64ff765f-c3bb-45fa-90ba-de8dfeaf6dab
- Kaya, L. (2016, August). NUMERICAL LOAD TESTING OF a GEOSYNTHETIC REINFORCED SOIL. Ph.D. dissertation. Retrieved September 21, 2023, from https://scholarspace.manoa.hawaii.edu/items/407d09dc-6943-4d86-9b69-4415dbc0c8fb
- Matsuoka, H., & Nakai, T. (1974). Stress-Deformation and Strength Characteristics of Soil Under Three Different Principal Stresses. Proceedings of the Japan Society of Civil Engineers, 1974, 59-70. doi:10.2208/jscej1969.1974.232_59
- Nakai, T. (1989, March). An Isotropic Hardening Elastoplastic Model for Sand Considering the Stress Path Dependency in Three-Dimensional Stresses. Soils and Foundations, 29, 119-137. doi:10.3208/sandf1972.29.119
- Nakai, T. (2013). Constitutive modeling of geomaterials : principles and applications. Taylor & Francis.

References

- Nakai, T., & Matsuoka, H. (1986, September). A Generalized Elastoplastic Constitutive Model for Clay in Three-Dimensional Stresses. Soils and Foundations, 26, 81-98. doi:10.3208/sandf1972.26.3_81
- Nakai, T., & Mihara, Y. (1984, June). A New Mechanical Quantity for Soils and its Application to Elastoplastic Constitutive Models. Soils and Foundations, 24, 82-94. doi:10.3208/sandf1972.24.2_82
- Nicks, J., Adams, M. T., Ooi, P., & Stabile, T. (2013, August). Geosynthetic Reinforced Soil Performance Testing—Axial Load Deformation Relationships. FHWA. Retrieved September 22, 2023
- Newland, P. L., & Allely, B. H. (1959, December). Volume Changes During Undrained Triaxial Tests on Saturated Dilatant Granular Materials. Géotechnique, 9, 174-182. doi:10.1680/geot.1959.9.4.174
- Roscoe, K. H., & Burland, J. B. (1968, January). On the Generalised stress-strain Behaviour of 'wet' Clay. (E. plasticity, F. A. Leckie, & J. Heyman, Eds.) Cambridge University Press,.
- Shen, P., Han, J., Zornberg, J. G., Morsy, A. M., Leshchinsky, D., Tanyu, B. F., & Chen, X. (2019, June). Two and three-dimensional numerical analyses of geosynthetic-reinforced soil (GRS) piers. Geotextiles and Geomembranes, 47, 352-368. doi:10.1016/j.geotexmem.2019.01.010

Thank You